INVESTIGATION ON THE EFFECTS OF SEAWATER ON MECHANICAL PROPERTIES OF API 5L X70 STEEL PIPELINE WELDMENT

BY

GAMBO, Abdulrahman Bala

(PhD/SEET/2016/860)

A THESIS SUBMITTED TO THE POSTGRADUATE SCHOOL FEDERAL UNIVERSIY OF TECHNOLOGY, MINNA, NIGERIA IN PARTIAL FULLFILMENT OF THE REQUIREMENTS FOR THE AWARD OF THE DEGREE OF DOCTOR OF PHILOSOPHY (PhD) OF ENGINEERING IN MECHANICAL ENGINEERING (INDUSTRIAL AND PRODUCTION ENGINEERING)

DECEMBER, 2022

ABSTRACT

Corrosion has been classified as a major threat to structures in marine environments leading to pitting, surface defects and subsequent failures. There is still a significant use of oil and gas pipeline which remains the only transportation medium for oil and gas products. These pipelines are classified according to their strength, chemical composition and the areas of application. There is a need to investigate the mechanical properties of welded pipeline operating in seawater. In this research, tensile, fracture, compression and hardness properties of API X 70 steel pipeline was investigated in natural seawater using a developed corrosion rig equipped with a chiller. The rig was developed using locally sourced materials. Tests were carried out using tensile, charpy, compression and hardness samples that were extracted from parent, weld and heat affected zones (HAZ). The fracture surfaces of the sample were analysed using scanning electron microscope (SEM). The coefficient of performance of the chiller was determined to be 3.58. In air, the mean yield strengths for parent and welded materials were found to be 560 Mpa and 578 Mpa respectively while the corresponding tensile strengths were determined to be 634 Mpa and 674 Mpa respectively. In seawater, the mean yield strength for parent and weld materials were obtained to be 428 Mpa and 416 Mpa and the corresponding tensile strengths were determined to be 512 Mpa and 529 Mpa respectively. Charpy energy values were higher in parent than in HAZ and with weld materials having the lowest energy. The absorbed energies in the specimens were relatively lower in seawater than those tested in air. The effect of seawater was also applicable to the reduction in compressive stresses of the material. The hardness value of the HAZ decreases from the region closer to the weld towards the parent material. The highest hardness of 239 HV value was obtained in weld, while the minimum harness of 196 HV was obtained in parent material. Fracture surfaces of the specimens showed the combination of brittle and ductile failure mechanisms. The effect of seawater corrosion reduced the tensile properties of parent and weld materials by factors of 1.2 and 1.3 respectively. Environmental reduction factor of approximately 2.0 was obtained in charpy parent, weld and HAZ materials. Seawater also reduced the compressive properties of parent and weld materials by factors of 1.7 and 1.8 respectively. Consequently, the study provided a novel approach of establishing mechanical properties of API 5L X70 steel plates at parent, weldment and heat affected zones in air and seawater for optimum pridiction of corrosion failure of pipelines and their prevention strategy. Design parameters were also established for the development of a new laboratory-scale corrosion rig for the API 5L X70 steel plates.

TABLE OF CONTENTS

LIST OF TABLES

LIST OF FIGURES

LIST OF PLATES

CHAPTER ONE

1.0 INTRODUCTION

1.1 Background to the Study

The global demand for transportation of resources such as oil and gas is rapidly increasing regardless of the challenges being faced in the oil and gas industry. The commonly used transportation media for these resources are pipeline structures. However, corrosion induced failure is generally considered as one of the most critical failure mechanisms in pipeline steels due to various types of environment and loading scenarios where pipeline structures operate.

The failure mechanisms coupled with environmental influence in the structures are site dependent and the understanding of the degree of damage that could be caused by these environments is an important factor that should be considered by operators and design engineers in order to ensure that the structures satisfy their design requirements. Corrosion is an empirical study which cannot be fully understood without app82ropriate experimental tests. Therefore corrosion has been generally considered in the oil and gas industry with respect to the capital expenditure (CAPEX) and operational expenditure (OPEX) as well as health, safety and the operating environment (HSE) (Kermani and Harrop, 1996).

Corrosion can significantly influence the cost of the materials from the design stage and it was mentioned that corrosion induced failures constitutes about 25% of the failures that occur in the oil and gas industries (Kermani and Harrop, 1996). From the investigations between 2010 to 2019, it was reported by the United States Department of Transportation (United States Department of Transportation, 2019) that out of approximately 6298 events that occurred, there were approximately 140 fatalities, about 565 injuries, over 920 fire outbreak cases, 320 cases were associated with explosions, over 5 billion USD was associated with damage to properties, and approximately

35,992 people left their residences as a result of pipeline failure. Recently, it was also reported in (Kelso, 2020) that the corrosion-related incidents that occurred since 2010 was reported to be 1037 cases associated with gas distribution lines and gas transmission. Also, the costs of yearly damages relating to corrosion in oil and gas industries were reported to be 1.372 billion USD, 320 million USD, and 463 million USD for surface pipeline infrastructure costs, capital expenditures, and downhole tubing expenditures (Popoola *et al.,* 2013). Therefore, it is important for pipelines design Engineers to optimize their designs and also engage proper monitoring techniques adequate corrosion failure management strategies for pipelines in operation.

The increase in demand of oil and gas requires greater supply of the products over long distances that is between the reservoir and the demand centres (Wang *et al.,* 2014). In the oil and gas industry, pipelines with various diameters and thicknesses are being used depending on the site, external loadings and operating pressure. The X80 pipelines which are usually fabricated are commonly used due to their high strength and toughness (Wang *et al.,* 2015). However, the need to use higher grade steels such as X70, X80 and X100 for high transmission efficiency and lower construction costs is becoming most apparent. The most commonly used pipeline steels globally are API X52, X60, X65, X70, X80. It is also evident that most pipeline networks in Nigeria are fabricated using X55 and X60 which are lower in grade compared to X70 steel. The earlier pipeline C-Mn steels are mostly the X42 and X52 grades with higher carbon content (Vesga Rivera, 2014). The newer pipeline steels are fabricated with lower carbon content in order to enhance weldability, toughness and strength. X100 steels are not commonly used in operation probably due to cost implications as well as their design which is specific to arctic regions. The X70 steel grades are manufactured by the

addition of other elements and improved manufacturing processes such as welding compared to previously-used lower grade steels. The welded sections of the pipelines are more prone to damage due to residual stresses and possible fabrication defects. However, most of the works found in the literature have not adequately studied the damage mechanisms in the weld and weld heat affected zones (HAZ). Corrosion of pipelines has always been an important topic in the oil and gas industry because of its harmful effects on the component life. It should be mentioned that several corrosion prevention measures have been developed in order to reduce the effects of corrosion in pipelines coupled with the reduction in costs being incurred in the management of corrosion related failures. Types of corrosion prevention measures are discussed in chapter 2. However, irrespective of the corrosion protection measures, there are unplanned situations such as losses of coating or poorly designed cathodic protection systems. It is therefore necessary to investigation the real effects of corrosion in pipelines so that these structures can be designed for optimal operation conditions, in order reduce significantly the large amount of money spent on repair or replacement of pipelines that are damaged by corrosion. Hence, in this research, the corrosion induced failure mechanisms in the X70 steel weldment was investigated in appropriate environments. Parent materials, weld and heat affected zones materials will be tested. Attempt was made to replicate the real onshore environment in a laboratory. Relevant corrosion induced failure tests such as tensile, fracture, compression and degree of corrosion degradation was carried out.

1.2 Statement of the Research Problem

Pipelines are generally prone to failure due to the types of load and the nature of the environmental induced damages they experience in service. Pipeline corrosion is one of the challenges facing the oil and gas industry. These pipelines are sections made from different grades of steels such as X70, X80 and X100 steels. However, studies have shown that the failure mechanisms in X70 steels particularly at the welded sections have not been adequately investigated (Aliu, 2012). These mechanisms include tensile properties, impact properties, compression properties and hardness properties that are accompanied by environmental influence on the steel sections. There is therefore a need to investigate the aforementioned failure mechanisms using X70 steel that is subjected to an environment representative of those experienced by the pipelines for a better understanding of the behaviour of pipeline structures that are designed with X70 steel (Akonyi *et al.*, 2020).

1.3 Aim and Objectives of the Research

The aim of this research is to investigate the effect of seawater on mechanical properties of X70 steel pipeline weldment.

The objectives of the research are to;

(i) Carry out the welding and mechanical characterization of the X70 steel pipeline plate

(ii) Develop a laboratory-scaled corrosion rig for testing pipeline materials in seawater.

(iii) Investigate the tensile, fracture, compression and hardness properties of parent and welded X70 steel pipeline plate in air and seawater.

(iv) Determine the environmental reduction factors by comparing the selected

Mechanical properties of the API X70 steel pipeline weldment in air and in seawater.

1.4 Justification for the Research

Pipelines are complex welded structures and are susceptible to corrosion induced damages to a degree which depends on the environment where they are located. Inspection and monitoring of these structures are important and expensive. The failure mechanisms in pipelines can be studied using cost effective representative materials in an environment similar to those experienced by pipeline steels. As such, the failure mechanisms of pipeline structures could provide design Engineers with adequate information regarding repair of faulty sections and the replacement of the damage ones if necessary.

1.5 Scope of the Research

In this work, the failure mechanisms/mechanical properties in pipeline steels were investigated in air and in seawater environments. The degree of corrosion degradation was measured. Tests were carried out on parent plates, weld regions and the heat affected zones. The corrosion induced failure mechanisms were limited to the effects of seawater environment on the mechanical properties of the steels. Welded X70 pipeline steel was used for investigation.

CHAPTER TWO

2.0 LITERATURE REVIEW

2.1 Theoretical Frame Work

The failure mechanisms coupled with environmental influence in the structures are site dependent and the understanding of the degree of damage that could be caused by these environments is an important factor that should be considered by operators and design engineers in order to ensure that the structures satisfy their design requirements. Corrosion is an empirical study which cannot be fully understood without app82ropriate experimental tests. Therefore corrosion has been generally considered in the oil and gas industry with respect to the capital expenditure (CAPEX) and operational expenditure (OPEX) as well as health, safety and the operating environment (HSE) (Kermani and Harrop, 1996).

Corrosion has been classified as a major threat to structures in marine environments leading to pitting, surface defects and subsequent failure. The background and mechanisms of corrosion induced failure in oil and gas pipeline structures have been discussed previously. However, some of the factors influencing corrosion failure mechanisms were discussed with respect to the available and relevant literature. The discussion was centered on studies conducted on marine corrosion (Kermani and Harrop, 1996).

2.2 Oil and Gas Steel Pipeline Grades

Irrespective of the irregularities in the prices of oil globally, there is still a significant use of oil and gas pipelines which remains the only transportation medium for oil and gas products. These pipelines are classified according to their strength, chemical composition and the areas of application. Pipelines are supplied in range of thicknesses

with each specific to the areas of application. With increasing demand in the use of steels globally, steel manufacturers now use advanced manufacturing techniques with a view to reducing weight and costs as well as improving mechanical properties. Pipelines are classified according to the American Petroleum Institute (API) and this includes API X42, X52, X65, X 70, X80, X100 and X120. (Vesga Rivera, 2014). Later pipeline steels grades are often manufactured by the reduction of carbon content and the addition of alloying elements such as elements (V, Nb, Ti, B). It was also reported by (Mustapha, 2010) that the addition of alloying elements such as C, Si and Mn to steels could enhance their strengths by the formation of martensite and bainite Pipeline steel grades are used subject to the specific area of application and the environments. For example, API X70 in shipping industries, oil storage tanks and temporal bridges for road construction aside it usage for oil and gas products (Ike, 2018). The highest grade of pipeline steel that could be manufactured with pearlite-ferrite microstructure without compromising weldability is the X70 steel grade (Hillenbrand *et al.,* 1999). The variation of microstructure of some of the API steel grades had shown that X70 contains ferrite-pearlite matrix, X80 contains ferrite-bainite and X100 contains the bainite microstructure as shown in Figure 2.1.

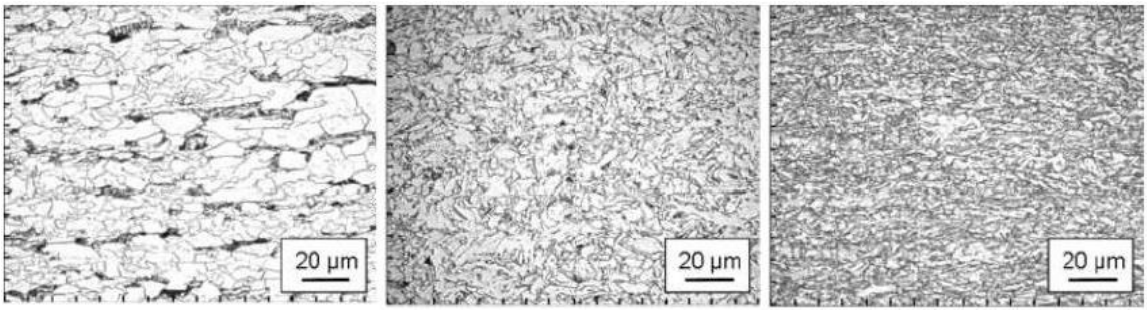

(a) (b) (c)

Figure 2.1: Microstructure of (a) API X70 (b) API X80 (c) API X100 steels (Hillenbrand *et al.,* 1999)

Idokoh (2016), discovered by using optical microscope and Transmission Electron Microscope (TEM) that X70 steel base plate has equiax ferrite grains while the welded joint revealed microstructure acicular ferrite and fine bainite grains, while similar grain types was also reported for X70 steel in (Omale *et al.*, 2017). The Pipeline steels produced from 1965 to 2008 with corresponding composition of carbon and alloying elements is shown in Figure 2.2 where it can be seen that there is reduction in the carbon content of the steels with respect to the addition of other alloying elements in order to enhance their properties. Therefore, improved manufacturing process that will enhance mechanical properties has necessitated the recent use of higher grades of pipeline steels which include X60, X65, X70, X80, X100 and X120 (Vesga Rivera, 2014), as oil and gas transportation media.

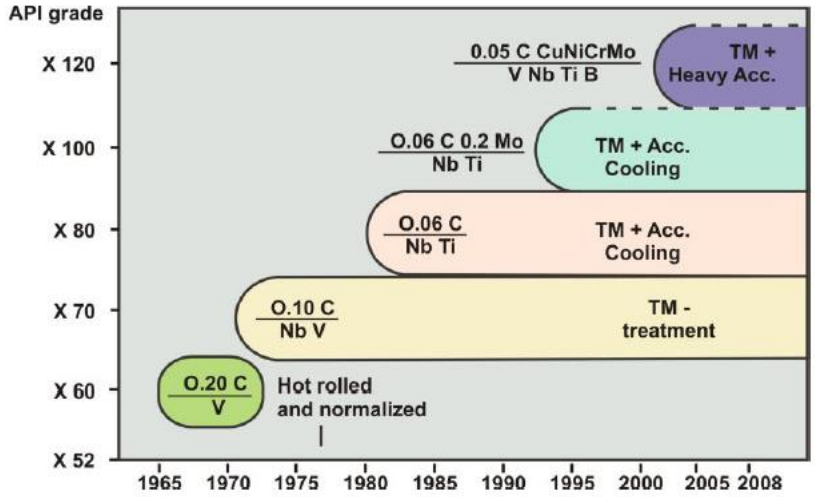

Figure 2.2: Variation of material composition for API steel grades (Hillenbrand *et al.*, 1999)

The typical composition of an API X80 and API X70 steels are shown in Tables 2.1 and 2.2. The composition pipeline steel may vary due to test environment and equipment.

Table 2.1: Chemical composition of X80 pipeline steel (Wang *et al.,* 2015)

Elements:	C	Si	Mn	P	S	Ni	Mo	Cu
% Composition:	0.07	0.30	1.77	0.02	0.005	0.22	0.21	0.22
Elements:	V	Al	Nb	Fe				
% Composition:	0.06	0.06	0.05	97.02				

Table 2.2: Chemical compositions of sample API X70 Steel (Ike, 2018)

Elements	%C	%Fe	%Si	%Mn	%Cr	%Mo	%Ni	%V	%Cu	%Al	CE
Base metal	0.05	97.73	0.210	1.510	0.240	0.118	0.07	0.021	<0.002	0.048	0.38

The type of manufacturing techniques, chemical compositions and the associated mechanical properties that are required for oil and gas pipelines have been mentioned according to the specifications of the American Petroleum Institute (API). However, due to long distances that are usually covered by pipelines, the most globally recognized method used for their fabrication is welding. The techniques have been categorized as the welding carried out in without the use of filler material which are termed continuous welding, electric welding and laser welding; and welding carried out using filler material, which includes (submerged-arc welding (SAW), gas metal-arc welding (Sharma and Maheshwari, 2017). The SAW process has proved useful for the fabrication of pipelines and pressure vessels longitudinal and circumferential butt weld joints. Submerged-arc welding process is schematically shown in Figure 2.3, where the filler material either in solid form or coiled wire driven mechanically, with the welding current being applied in the range of 300 to 1000 Amperes.

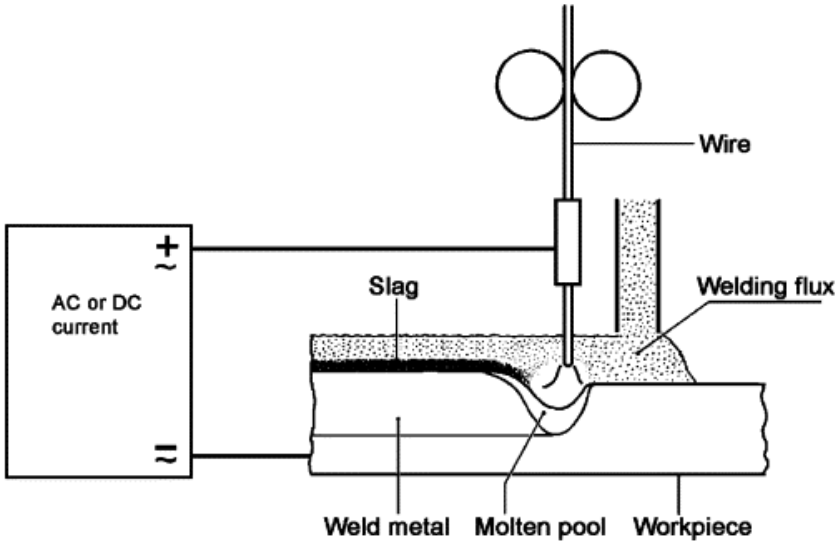

Figure 2.3: Submerged-arc welding (SAW) process (Naidu *et al.,* 2003)

However, regardless of the manufacturing technique used during pipeline production, they are susceptible to corrosion, stress corrosion cracking (Li and Cheng, 2008; Javidi and Horeh, 2014; Song, 2009). Corrosion fatigue and other forms of failure depending on the types of loads they experience as well as their locations. Corrosion in pipelines therefore plays a significant cost implication role in the oil and gas industries.

Most researches have focused mainly on internal corrosion induced by CO_2 and H_2S environments and this has also been confirmed in Wang *et al.*, (2015). A study was also conducted on corrosion of X100 steels in aerated carbonate solution by electrochemical method (Eliyan *et al.,* 2013). However, external corrosion in pipeline structure is a mechanism that cannot be neglected and only a few of such studies have been reported in the literature, therefore, studies relating failure due by corrosion particularly in pipeline steels that are used for deep water applications are important. Pipelines are usually coated but some unplanned conditions may set in during operation such as poor design of coating, loss of coating due to damages either during manufacturing or transportation of the pipelines. Therefore, the extent to which corrosion can influence

mechanical damages without corrosion protection or a free corrosion environment needs to be studied.

Marine corrosion in aerated NaCl solution was reported as the major cause of failure in X80 pipeline steel (Brondel *et al.*, 1999; Chen *et al.*, 2015; Ilman, 2014). A significant number of studies conducted on pipeline steels and other steels used for marine structures have considered corrosion induced fatigue failures. For example in Adedipe *et al.* (2015), it was established that crack growth in seawater environments is significantly higher than those reported in air environment. However, this discussion is beyond the scope of this research. Other forms of corrosion induced failure mechanisms in pipeline steels, particularly in X70 steel therefore need to be studied in appropriate environment for a better understanding.

2.3 Corrosion Mechanism

In corrosive environments particularly in seawater, corrosion is the deterioration of material by an electrochemical reaction which occurs by the release of electrons form the material into the environments through the process of oxidation (Adedipe, 2015). However, the extent of the deterioration coupled with the loss of wall thickness may depend on the material and environment. A typical example of corrosion reaction particularly damages that occur under free corrosion conditions is described from equation (2.1) - (2.3).

$$Fe \rightarrow Fe^{2+} + 2e^{-} \tag{2.1}$$

$$H_2O + \frac{1}{2}O_2 + 2e^{-} \rightarrow 2OH^{-} \tag{2.2}$$

$$Fe^{2+} + 2OH^{-} \rightarrow Fe(OH)_2 \tag{2.3}$$

Equation (2.1) explains the process of anodic dissolution which occurs in seawater corrosion when electrons are released from steel by oxidation. A further explanation of the process of anodic dissolution can be found in Austin and Julian (1994) and Myers (1998) works. Different types of corrosion have been explained in the literature (Shifler and Denise, 2005). The main focus of this research is to address the mechanical related failures due to the interaction of the material with seawater environment but not the mechanisms of corrosion in detail. Some of the types of corrosion are discussed as follows.

2.4 Types of Corrosion

Corrosion is a wide area of research and therefore corrosion induced failure testing depends on quite a number of variables, and it may not be cost effective to investigate on the variables during experimental tests. Particular variable and environment depend on the type of information desired by the investigator. However, understanding the significance and the interaction of the variables involved in corrosion failures informed the decision on how to structure laboratory experimental tests that will represent the service condition optimally. Types of corrosion have been classified as uniform corrosion, localized corrosion and stress corrosion or environmentally assisted cracking. Localized corrosion can be classified as pitting, crevice corrosion, galvanic corrosion, microbial, erosion corrosion, corrosion fatigue and stress corrosion cracking (Shifler and Denis, 2005; Kalantzis, 2014).

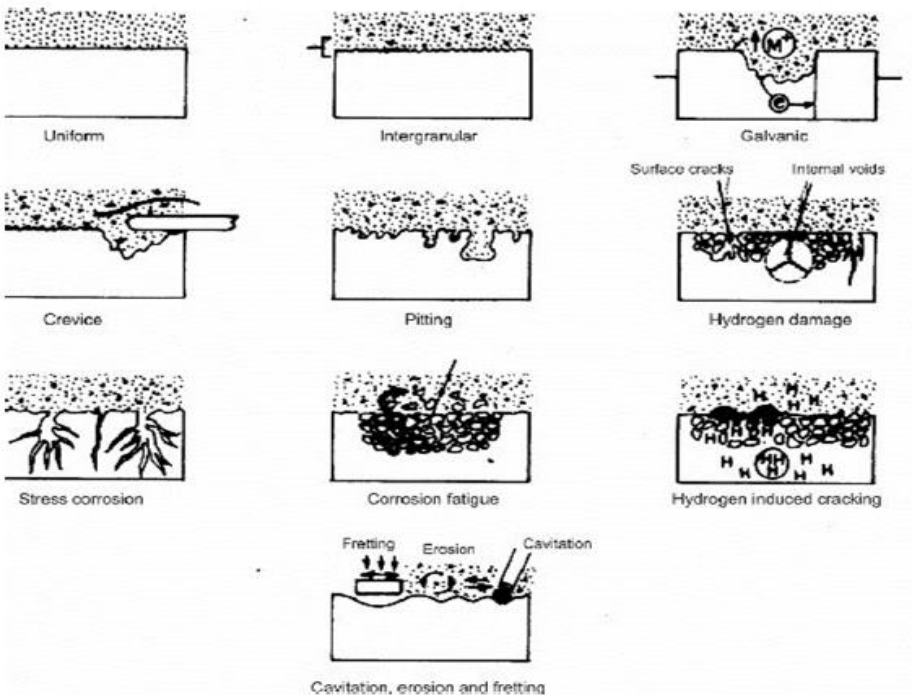

Figure 2.4: Types of corrosion (Cicek and Al-numan, 2011)

Various types of corrosion are shown in Figure 2.4. These are discussed briefly. Uniform corrosion as the name implies is the most common corrosion which is uniformly distributed on the metal surface. Uniform corrosion in pipelines is identified as an electrochemical reaction that destroys the entire surface of the material leading to thinning loss of thickness of the pipeline (Kalantzis, 2014). In localized corrosion, the corrosion effect is restricted to a particular area on the metal and this is why it is termed a localized damage. Localized corrosion may be difficult to predict and estimate due to the stochastic nature and severity subject to environmental effects. Pitting is a typical type of localized corrosion. Pitting corrosion depends on electrochemical potential, microstructure and chemical composition of the material, pH, composition of the electrolyte and temperature (Revie, 2000). Pitting corrosion starts when it penetrates the protective oxide film that is either applied or formed naturally on the surface of the material which is intended to act as corrosion protection (Wang *et al.,* 2015). As the film deteriorates, oxidation increases due to the presence of oxygen and this increase the

potential for pitting on the material surface as shown for stainless steel in Figure 2.5, where it can be seen that $Fe(OH)_3$ is deposited on the surface of the material. In stainless steels, the deposits n the surface is usually accompanied by elements such as chromium, nickel and molybdenum. Pitting corrosion is common to metal that form protective on their surfaces and which do not react easily with their environments. These include stainless steel, aluminium, copper and nickel based alloys. However, the mechanism shown in Figure 2.5 may depend on the material and environment and a further discussion of this is beyond the scope of this research. In marine environments, pitting corrosion may significantly reduce the significance of the protective layer in steels.

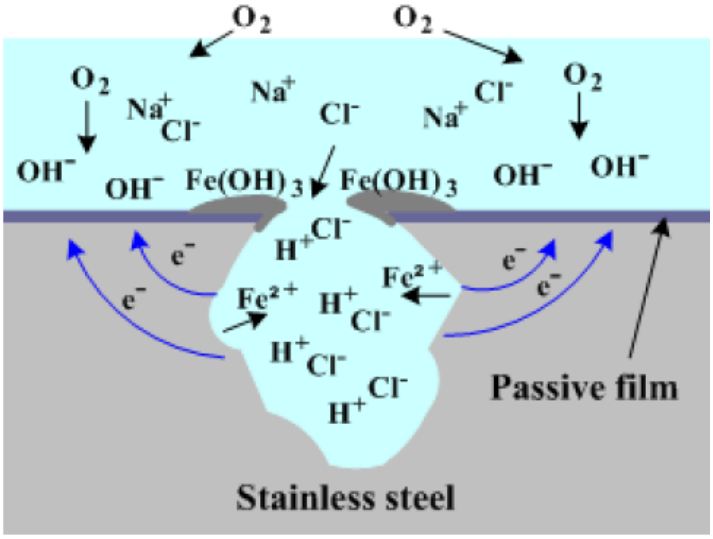

Figure 2.5: Corrosion pit mechanism in stainless steel (Kalantzis, 2014)

In pipelines, seam weld corrosion has been identified as one of the most critical forms of failure. In welded structures, damages either by corrosion or other loading scenario starts from the weld heat affected zones (HAZ) and progress into the parent material (Johnson *et al.*, 1978). This is because of the presence of weld induced residual stresses accompanied by heat input and composition of the filler material that was employed in welding. The extent of the corrosion induced damages may vary from material to

material. It was reported by Adedipe, (2015) that the appearance of corrosion surfaces of HAZ materials are significantly higher than those in weld and parent materials. This may be because of the material variability in HAZ microstructure.

Crevice corrosion can be described as another form of localized corrosion which occurs at the joints and it involves both initiation and propagation stages depending on the environment. In the former, some discrete areas are developed with the crevice leading to oxygen reduction. While in the latter, the loss of oxygen is accompanied with acidification and chloride ion build up (Sedriks, 1996). In galvanic and erosion corrosion the passive layers that are susceptible to corrosion can be attacked thereby exposing the steel to the effect of corrosion. For example, in copper-nickel alloys, loss of the protective layers may result in the interaction of the material with the environment causing the enhancement of galvanic type of corrosion. More specifically, in erosion corrosion, the damage is characterized by flow related mechanical removal of protective layers resulting in corrosion rate either by electrochemical or chemical process (Shifler and Denis, 2005). The characteristic feature of the surface affected by erosion corrosion usually exhibits a shallow type pit having a similar shape with the direction of the flow. However, in galvanic corrosion, the damage mechanisms usually occur when two dissimilar metals have different potential are under electrical contact in an electrolyte such as water. This is shown in Figure 2.6.

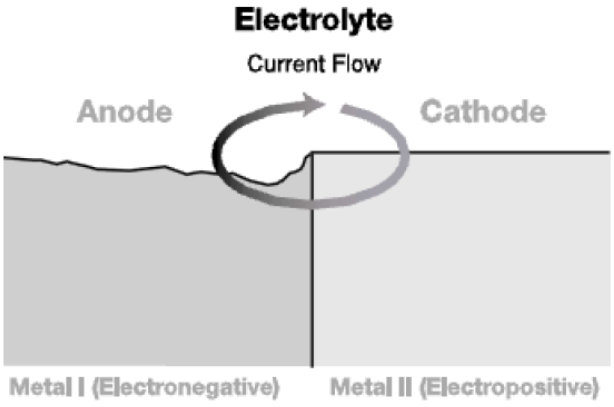

Figure 2.6: Mechanism of galvanic corrosion (Kalantzis 2014)

In Microbial Induced Corrosion (MIC), the damage mechanisms are influenced by the activities of microorganisms, particularly the bacteria that are present in the corrosive environment. This type of corrosion is common to pipelines and has been explained by (Little and Lee, 2007) as the formation of bio films by the activity of microorganism on the steel surface. MIC can also be enhanced by the presence of water, pitting and crevice corrosion. A typical feature of microbial induced corrosion can be seen in Figure 2.7. The most common bacteria resulting from MIC in pipeline structures are the Sulphate Reducing Bacteria (SRB) and CO_2 reducing (Beech and Sunner, 2004).

Figure 2.7: Microbial induced corrosion (Kalantzis, 2014)

Environmental induced cracking such as stress corrosion cracking, corrosion fatigue and hydrogen embrittlement. In stress corrosion cracking, the failure is enhanced by the combination of tensile stress or monotonic stress and the corrosive environment with both working simultaneously. It can be referred to as a static type of failure. Corrosion fatigue as the name implies is a critical form of failure which occurs due to fatigue load and the corrosive environment. This type of failure is peculiar to marine structures and a typical example of experimental investigations on corrosion fatigue failures can be found in Adedipe (2015).

Hydrogen embrittlement is a form of failure which results in brittleness of steels when they come in contact with hydrogen (Raymond, 1988). This type of failure is mostly common in high strength steels and steels that are under cathodic protection in marine environment. Hydrogen embrritlement occurs when there is over protection or when the CP is not properly designed. The mechanism of hydrogen embrittlement in association with CP of different potentials has been explained by Scott *et al.*, (1983).

2.5 Factors Influencing Pipeline Corrosion in Marine Environment

Corrosion of pipelines in marine environments is a type of damage which results in surface roughness of the steel, crack initiation from pits and propagation and eventual failure if the structure is not monitored and repaired or replaced as the case may be. Corrosion of pipelines in seawater environments depends on several factors. These include temperature, dissolved oxygen content, salinity, chemical composition of the material, seawater chemistry, pH, types of microbiological organisms, geometry of the pipeline and surface roughness (Shifler and Denis, 2005). However, the factors that are responsible for corrosion in marine environment depend on the material and environment. In immersed ship hall steel, the environmental factors influencing corrosion after coating loss includes seawater temperature, concentration of dissolved oxygen, pH and salinity (Garbatov *et al.*, 2014). The contributions of these factors to rates of corrosion are discussed next.

Corrosion of steel immersed in seawater increases with an increase in temperature of the seawater. Seawater temperature is the major factor controlling the duration different stages of corrosion in steels. Corrosion is time dependent; this is probably why temperature could either be increased or the corrosion media could be acidified in accelerated tests in order to mimic the type of corrosion damage scenarios in structures

that are in seawater environment. Temperature changes with season and water depths; and this may also have significant effect on corrosion in pipelines. Dissolved oxygen also has a major influence on corrosion rates and as the seawater temperature increases, the solubility of oxygen reduces. Biology activity also increases with increase in temperature of seawater and it has been mentioned that most bacteria activity in seawater are pronounced at the temperature of 15 to 45 ^{o}C (Dexter, 2003). In alloys having protective film on their surfaces, corrosion attack may be reduced but if there is oxygen variation to a level where the protective films are attacked, a localized type of corrosion such as pitting may occur. Seawater pH outside the range of 5-10 could also increase the rates of corrosion (Garbatov *et al.,* 2014). The pH of seawater that is mostly used for experimental investigation is in the range of 7.8 to 8.2 (Garbatov *et al.,* 2014).

Material composition is another factor influencing pipeline corrosion in marine environment. This is why information about the material properties is important so as to establish that material used for experimental investigations meet the API requirements (Leonardo *et al.,* 2014). Leonardo *et al.,* (2014) investigated the mechanical and fatigue crack behaviours of X60 and X70 steel used in the transportation of iron ore. All the tests such as impact, tensile, crack tip opening displacement (CTOD) as well as fatigue crack growth tests were conducted in air at room temperature. It was found that the X70 steel performed better that X60 steel considering all the tests that were carried out. It was also suggested that X70 steel could be replaced by X60 steel when considering pipeline steel for iron ore transportation. However, no effect of corrosion enhanced damage was investigated in the work. The chemical composition of the X70 steel used for the experimental investigation as reported by Leonardo *et al.,* (2014) is shown in Table 2.3.

Table 2.3: Chemical composition of API-5L X70 steel (wt%)

Elements:	C	Si	S	P	Mn	Ni	Cr	Cu	Al
% Composition:	0.109	0.239	0.004	0.023	1.536	0.011	0.024	0.011	0.026
Elements:	V	Ti	Nb	Fe					
% Composition:	0.045	0.016	0.045	97.1					

Source: Leonardo *et al.* (2014)

Salinity of marine water depends not only on site but also on water depths. The salinity of seawater at the surface was reported to vary between 32 to 37.5% (Shifler and Denis, 2005). The variation in salinity has an influence on the level of corrosion in steels. If salinity is increased, the production of chloride also increases, resulting in pit development and crevice corrosion (Shifler and Denis, 2005). Formation of calcareous deposit is another factor responsible for the corrosion of steel structures in marine environment. Calcareous deposits occur both at the sea surface as well as in deep waters and their action increase under high cathodic protection systems. Biological organisms in water produce both bacteria and macro algae and these formations affect can the corrosion of metals by influencing the corrosion level of the environment through the anodic and cathodic process occurring as well as influence the levels of calcareous deposits formed on the surface. Effect of surface finish and material are other important factors that could influence corrosion in metals. Materials vary in microstructure; therefore corrosion attack may be massive in one material than the other. Surface finish which could be due to either fabrication errors or preexisting defects which are introduced during transportation and installation could influence the degree of stress concentration and corrosion attack especially at welded sections.

2.5.1 Seawater environment and corrosion testing

Seawater is an environment that cannot be reproduced in the laboratory completely but can be simulated as close as possible. Seawater varies from zone to zone depending on the chemical composition, pH and temperature. Seawater has different environmental zone and this includes splash zone, tidal zone, mud zones, shallow water, and deep ocean zone. Each of these zones has different influence on corrosion and pipelines located in each zone require different levels of protection. The environmental influence of each zone on corrosion is described in Shifler, (2005). Seawater covers about 71% of the surface of the earth and seawater contains about 3.5% of sodium chloride. This is why a larger concentration of sodium chloride is used when carrying out experimental investigations on corrosion induced damages.

Corrosion testing depends on the investigators need and it is not cost effective to include all the variables affecting corrosion during testing due to the interaction of these variables. Each test is designed based on a study of the environmental factors and types of load that are experienced in a particular site. Due to cost implication and time constraints, accelerated tests are carried out in the laboratory and are applied to predict corrosion failure of structures in service. Natural seawater is used as the test media in most cases and is collected directly from the sea. Synthetic seawater is also used for corrosion testing; the preparation of synthetic seawater can be found in ASTM D1141 (ASTM D1141, 2008). A type of laboratory based corrosion test that will majorly be considered in this study is the immersion or soaking test. In this test, the test samples are immersed in seawater for a particular period. The seawater can be replaced occasionally, circulated or uncirculated depending on the method adopted. The material

can be brought out for testing after soaking and be examined for weight loss, physical changes as well as mechanical or failure related test. Other laboratory test includes electrochemical, erosion corrosion, stress corrosion cracking, hydrogen embrittlement and corrosion fatigue tests. However, in this research, only the immersion test will be considered by soaking specimens in a circulated seawater media.

2.6 Corrosion Protection in Offshore Pipelines

As mentioned previously, coating is regarded as one of the corrosion protection measures for offshore pipelines. Cathodic protection systems are also used as backup and are also most effective at the splash zones due to the higher corrosion rates that are specific to splash zones. Cathodic protection system will be discussed in another section. However, coating may experience failure in service and this may lead to significant levels of corrosion. It was mentioned by Norman and Agent (Norman and Argent, 2007) that offshore pipeline coatings experience failure modes irrespective of cathodic protection systems that are employed, resulting in external corrosion coupled with cracking, microbial corrosion and cathodic protection shielding. The effect of cathodic protection failure was also reported to have resulted to high corrosion rates due to the coating loss (Roche, 2005).

Most of the corrosion protection measures such as cathodic protection are expensive and require significant efforts in developing them (Ijaola *et al.*, 2020). Aluminium coatings were identified for use in pipelines operating in seawater environment; but due to long term corrosion protection that is peculiar to pipelines, aluminium coating may not be suitable due to the associated generated flaws and pores that could facilitate coating loss (Chen *et al.*, 2014). A type of corrosion failure resulting from coating loss is shown in Figure 2.8. The most areas of the pipelines that are more susceptible to corrosion due to coating losses are the risers which are flexible or rigid pipes that serve

as medium of transportation of fluids for the seabed to the surface facilities. Risers are always protected by thick coating due to the levels of corrosion that are experienced during operation. Risers are joined together by welding and these welded joint are potential spots for crack initiation and propagation due to stresses that are produced at the circumferential weld. In the event of coating loss, the rates of propagation of damages in the welded sections are expected to increase significantly.

Figure 2.8: External corrosion in pipeline (Kalantzis, 2014)

Some of the commonly used coating systems in pipelines have been outlined as tars and asphalt enamels, one to two layers of polyethylene, fusion bonded epoxy (FBE), three layers of polypropylene (3LPP), glass reinforced plastics are rubber coatings (Kalantzis, 2014). However, these coating systems and their mechanisms are not discussed in this research.

2.6.1 Cathodic protection

Cathodic protection (CP) systems are used as backups to coating in pipelines. They are two major types of CP: sacrificial anode type and the impressed current type. In sacrificial anode, a metal that is more negative in potential or more active is made the anode while the metal to be offered protection is made the cathode. Electrons move

from the sacrificial anode to the cathode leading to corrosion of the anode. In most cases, metals that are higher in the electrochemical scale are usually offered as anode to the metals that are below them. For example, when protecting steels against seawater corrosion, any of magnesium, zinc and aluninium can be offered as anodes.

In the impressed current, the system is constructed using graphite electrodes on the steel in seawater. The system is then monitored by a DC power supply which supplies current with reference silver/siver chloride (Ag/AgCl) electrodes. In the Ag/AgCl reference electrode, there is an interaction between silver (Ag) metal and its salt silver chloride AgCl. Electrical potential is therefore measured and passed to the control panel with the intention of either reducing or increasing the outputs to the anodes. The impressed current therefore reduce the effect of the corrosion, thereby measuring the steel to electrolyte potential so as to determine the level of corrosion protection that is being offered to the steel. Cathodic protection systems are not considered as part of this research as mechanical tests will be conducted on steels samples that have experienced a free corrosion condition.

2.7 Review of Related Literature on Mechanical Characterization of Pipeline Steels

Grades and Corrosion Failures

Corrosion related failures are usually carried out on materials that are soaked in corrosive environment for a specific duration. The mechanical/failure tests that were carried out in this work are tensile test, impact test, and hardness test. In tensile testing, the sample is subjected to a controlled tension until failure occurs. Impact test is carried out to determine the amount of energy absorbed by a material during fracture. During compression tests, the material experiences opposing forces that are applied from both directions. Hardness tests are usually carried out by applying the relevant force to the

specimen through an indenter on the hardness testing machine in order to determine the hardness property of the material.

Pipeline steels grades are expected to reveal different mechanical properties due to material variability in terms of chemical compositions and manufacturing procedure. This was confirmed by a study carried out in Cheng and Xue (2011) where the mechanical properties and microstructure of X70 and X80 pipeline steels were compared. The mechanical characterization results were found to be influenced by variation in the steel properties. A comparison was made in (Leonardo *et al.,* 2014) with respect to the microstructure and mechanical properties of X60 and X70 pipeline steel. The X70 steel was found to exhibit better mechanical properties in terms of tensile, impact and hardness tests. The results were explained by the lower carbon content of X70 and other alloying elements. This is probably why steel manufacturers now reduce carbon composition and steels and optimize other alloying element in order to enhance weldability and strength.

However, regardless of the material type an investigation had revealed that the pipeline laid in the 1980s. Aliu (2012) revealed that most pipeline steels belong to the class of High Strength Low Alloy Steel irrespective of mechanical tests (charpy and tensile). Better mechanical properties compared to lower grades of pipeline steels were also revealed in a study carried out by (Muneer *et al.,* 2015). It appears in the literature that the mostly used pipeline steel is the X70 grade probably due to its performance in several areas of application such as shipping industries, oil storage tanks and temporal bridges for road construction as mentioned previously. It was also mentioned that longitudinal submerged arc welded fine-grained steel fabricated with X70 and X80 are the most commonly used pipeline steel for transportation of oil and gas products (Fan *et al.,* 2020).

As mentioned previously most studies reported in the literature on pipeline corrosion have reported failure due to mechanical related testing. An example of such study was conducted on ship hull steel (Garbatov *et al.*, 2014), where tensile tests were carried out on small scale specimens that were extracted from the corroded section of a box girder having a yield stress of 235 MPa and tensile strength of 400 MPa. The corrosion of the section was achieved by soaking it in real seawater in order to represent the type of corrosion damage similar to the ones in the real ships. The appearances of the corroded tensile sample and the corroded box girder are shown in Figure 2.9. The black elliptical sign on the box girder is the location where the samples were taken from.

Figure 2.9 left: corroded tensile sample, **Right:** corroded box girder (Garbatov *et al.*, 2014)

From the tensile investigation, the following properties were obtained; yield stress, tensile strength, fracture toughness, and total uniform elongation. The box girder was exposed in the seawater for 3 months while the corrosion rate was facilitated by

increasing the seawater temperature as well as the oxygen concentration. The true stress-strain relationship that was obtained from testing is shown in Figure 2.10. It was found that the reduction in strength was noticeable in corroded samples having more than 20% degree of degradation. Further experimental details can be found in (Garbatov *et al.,* 2014).

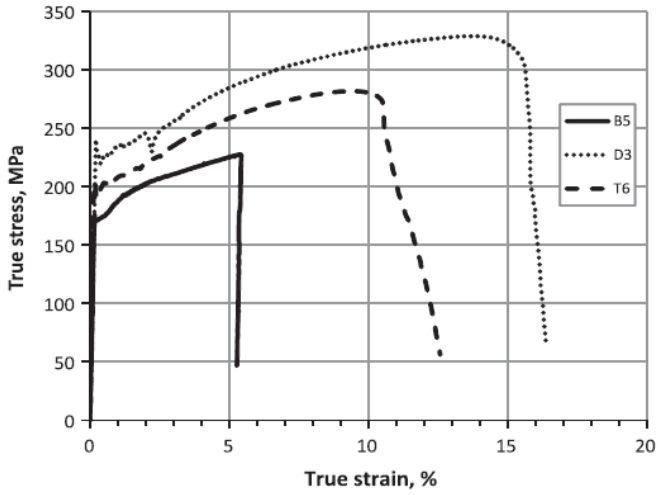

Figure 2.10: Stress-strain relationship for corroded tensile samples (Garbatov *et al.,* 2014)

The deteriorating effect of seawater was also shown in a study reported in (Ike et al. 2019) for 20.8 mm thick parent and welded API X70 steel, with the weld samples prepared using double V weld preparation manual metal arc welding (MMA) process in flat (1G) position. The samples were soaked in seawater for 12 weeks. The tensile strengths of the soaked specimens reduced by 10.5 % when compared with those tested in air. Similarly, the compressive strengths and the energy absorbed by the soaked specimens reduced by 18.7 and 37 % compared to specimens that were tested in air (under ambient condition).

Recently, a typical nature of corrosion related mechanical failure addressing tensile and fracture properties was investigated in Yang *et al.,* (2020) using seamless round steel

pipe with an outside of 25 mm and wall thickness of 1 mm; and subjected to accelerated electrochemical corroding environment with 5 % NaCl solution. The deteriorating influence of the corrosive environment is shown in Figure 2.11.

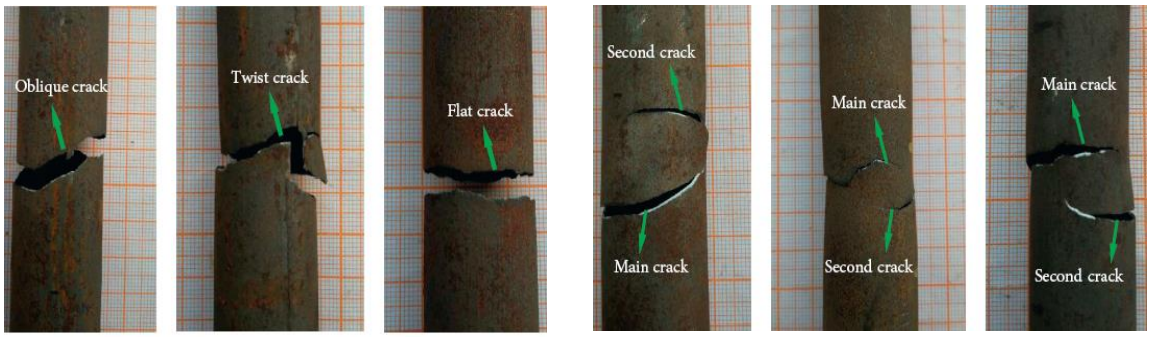

(a) (b)

Figure 2.11: Pipe failure due to (a) lower corrosion rates (b) enhanced corrosion rates (Yang *et al.*, 2020)

It can be observed that there are multiple crack related failure sites under accelerated corrosion compared to when corrosion rate is lower. This justifies the reason where corrosion related mechanical failure tests are carried out in the laboratory using simulated accelerated corrosion conditions in order to reduce experimental time compared to real effect of corrosion (measured in corrosion rates per year) which could take several years to manifest. The results represented in Figure 2.11 (Yang *et al.*, 2020) revealed that for corrosion rates of 10 % and 50 %, the corresponding yield and ultimate strengths of the corroded pipe were about 97 %, 76 % and 97 % and 75 % lower than those of parent pipes. The implication of this results is that for conservative design of pipeline in aggressive environment, the environmental reduction factor caused by the corrosive media need to be investigated.

Deteriorating effect of corrosion has also been shown in pipelines subjected to other corrosive environment aside seawater and NaCl. These include carbon dioxide environment (CO_2) and hydrogen sulphide (H_2S) environment. It is therefore expected that the behaviour of pipelines in these environments would vary due to their different chemical activities taking place. In (Vesga Rivera, 2014), mechanical and fracture properties of X60, X70 and X100 steels were compared by exposing them to SO_2 and H_2S impurities between 50 to 400 hours. Better mechanical properties in terms of hardness, yield and tensile strengths were revealed for X70 compared to X60 and X100 steels. It was found that the energy absorbed by X70 in both environments was higher than those absorbed by X100 and X60 steels. However, X100 steel revealed higher fracture energy than X60 steel. These results have also showed the better performance of X70 steel compared to other grades of pipeline steels regardless of test environment. However, the study did not consider the experimental of mechanical and fracture properties of specimens extracted from weld and HAZ regions. The implication of test conducted on the aforementioned regions could serve as reliable base line for estimating the lifetime and to decide monitoring routine of pipeline structures as it had been established in the literature that most failures originate from weld regions. Even with the corrosion protection measures such as coating that are now being employed for structures operating in marine environments, welded joints are susceptible to corrosion induced crack in the event of coating losses. Corrosion crack nucleation mechanism was investigated welded API X 65 specimens of dimensions 350 mm x 150 mm x 10 mm using natural seawater (Bai *et al.,* 2018). Microstructure, corrosion morphology and residual stress induced by welding were investigated using the specimens; and it was revealed that corrosion rate and morphology were significantly influenced by the

microstructure of the weldment (HAZ, weld and fusion zone) with respect to the presence of residual stresses.

The Mechanical and metallurgical properties of welded X80 steel pipeline that was welded using the submerged arc welding process was reported (Kim *et al.,* 2005). Hardness, fracture, bending and tensile properties of the samples were investigated in an air environment. The results were interpreted with respect to tensile and fracture properties of the material. However, environmental reduction factors were not considered in the properties due to corrosion damage. In this work, the experimental investigation carried out revealed environmental reduction factors of tests conducted on both corroded specimens and specimens that were not soaked in seawater.

2.8 Corrosion Rig for Testing of Pipeline Steel Materials

One of the main focuses of this research is to replicate the type of corrosion environment pipeline structures operate during their service periods. This can only be achieved experimentally by providing a similar corrosive environment in the laboratory. Hence, a corrosion rig was developed to achieve this. The development of the corrosion setup is described in chapter 3. In the next section, the major component of the corrosion rig is described with refrigerating systems due to their similarity in principle of operation.

2.8.1 Chillers

Chillers which are also referred to as refrigerating systems form the significant part of corrosion testing facility. They have similar principle of operation to refrigerators which primarily used for storage of food and drinks. They were designed with thermally insulated compartments and the compressor that transfers heat from the inside of the generating system to its external environment enable the reduction of the inside

temperature below room temperature. Chillers can be defined as refrigerating systems that uses vapour-compression cycle to chill water to a desired temperature for its use for a specific purpose. The working principle of a chiller designed to chill water from 10 ^{o}C to 20 ^{o}C is schematically shown in Figure 2.12.

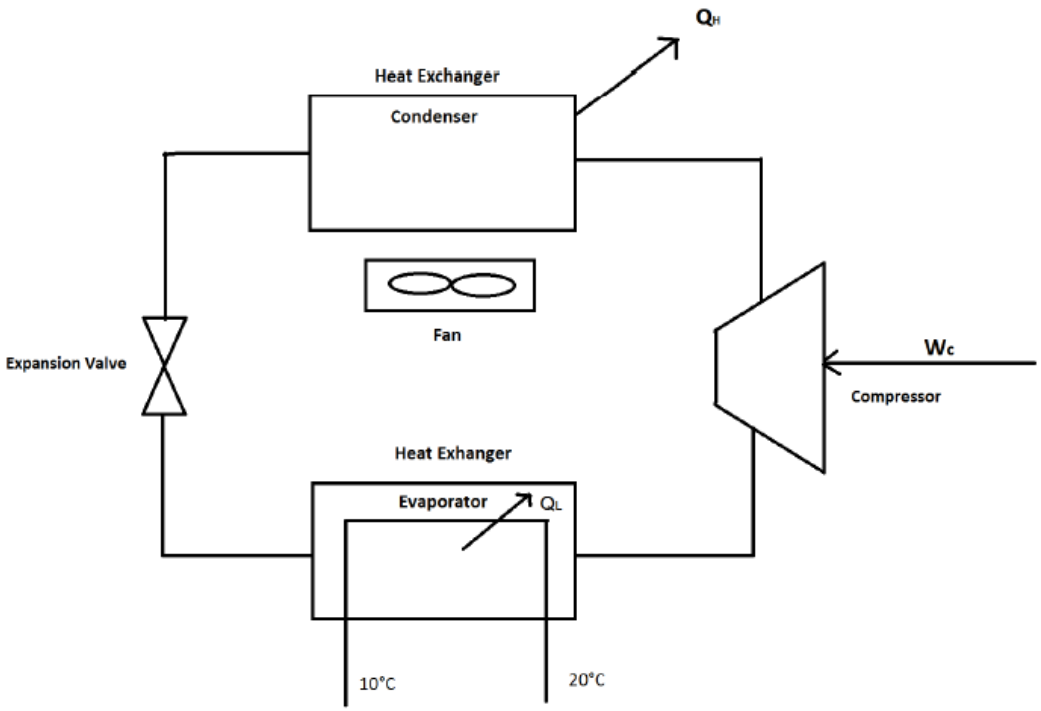

Figure 2.12: Working principle of a chiller (Ayres, 2013)

A typical example of a chiller that is similar to the one used in this research is the aquarium chiller which the inside is revealed in Figure 2.13. Aquarium chillers use vapour-compression operational principle for cooling. The major difference between the working principles of refrigerators and chiller is that the cooled water in chiller is pumped for a specific purpose unlike in refrigerator where cooled water, drinks and foods are retained in the compartment.

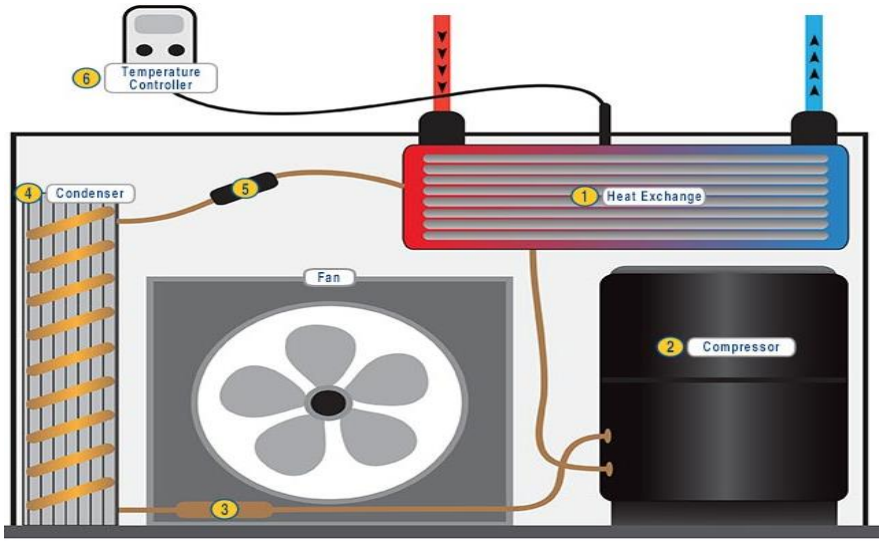

Figure 2.13: Aquarium Chiller

(Bolaji *et al.*, 2019)

The working principle of aquarium chillers is in two major stages, in stage one, water is pumped to the chiller and it enters the heat exchanger which is designed with coils contains refrigerant. Heat is transferred from the water to the refrigerant. The heated refrigerant is then compressed and it is changed from liquid to gas in the compressor; a pressure is therefore produced inside the compressor which forces the refrigerant into the cooling system as indicated in Figure 2.13. In the second stage, the refrigerant in form of gas moves from the compressor to the condenser by pressure. Air blows to the condenser through the fan which cools the refrigerant and heat is released to the environment in a similar manner as in car radiators. The refrigerant therefore changes to liquid in the condenser and it is passed through an expansion valve which reduces the pressure; and the rate of cooling experienced by the aquarium water is being controlled inside the heat exchanger or evaporator. An aquarium chiller is used during summer in the United Kingdom (UK) in order to control the temperature experienced by inhabitants of the aquarium. Apart from its use for cooling, aquarium chiller was used in the development of a corrosion fatigue set up during the testing of marine steel (BS355D) as part of the test programme of a major UK project (Adedipe, 2015). The

chiller was used to reduce the temperature of simulated seawater to a temperature representing that of the North Sea. Chillers are mostly designed for industrial use; however, as mentioned earlier, they have closely similar principle of operation as usual refrigerators that are used in homes. Refrigerators are designed with compressor, condenser, expansion valve or capillary tube and evaporator. Refrigerant in form of gas is compressed in the compressor to increase the temperature and pressure; the temperature of the gas is lowered in the condenser and changes to liquid. In the expansion valve, the pressure of the liquid refrigerant is reduced and it flows into the evaporator to cool the items in the cooling compartment while heat is transferred from the cooled area to the refrigerant to increase the temperature to a sufficient level to induce change of the liquid to gas; which flows back to the compressor (Khazrattul Bin Bani, 2008). A similar principle of operation as refrigerators is adopted in the design of the chiller that was used in this research. Most refrigerators and air conditioning system use vapour-compression cycle and this have been classified by four major stages; isentropic compression in a compressor, constant-pressure heat rejection in a condenser, throttling in the capillary tube or expansion valve and constant-pressure heat absorption in an evaporator (Khazrattul Bin Bani, 2008). Summarily, chiller is a single unit comprising of compressor, condenser, evaporator and expansion valve. The four major components of a chiller; compressor, condenser, expansion valve and evaporator are described in the following section

2.8.2 Vapour-compression cycle

i. Compressor: The major work of a compressor is to increase the power of the refrigerant and since the entire process is a closed loop, the vapour refrigerant at low temperature and pressure flows from the evaporator to the compressor and it is

compressed to a high temperature and pressure. The refrigerant is then discharged into the condenser under high temperature and pressure.

ii. Condenser: Condensers function as heat rejection device; they function as coolers to cool liquid or gas to a desired temperature. Condenser is made of coiled pipes inside which the refrigerant under high temperature and pressure is cooled, condensed and release heat into the surrounding environment.

iii. Expansion valve or capillary tube: As mentioned earlier, the principal function of the capillary tube is to perform the throttling process and it is also referred to as throttle valve. In the expansion valve the liquid refrigerant is passed at a controlled rate and with reduced temperature and pressure. A portion of the liquid-vapour refrigerant evaporates at the expansion valve while a larger portion of it is vapourised in the evaporator.

iv Evaporator: The evaporator is designed in a way that it accepts heat and it is made up of coiled pipes and it evaporates the liquid-vapour refrigerant, changes it to vapour refrigerant at low temperature and pressure. The schematic diagrams of a vapour-compression for refrigerating unit are shown in Figure 2.14.

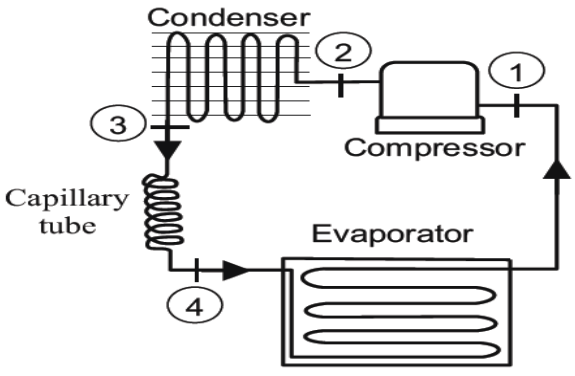

Figure 2.14:Vapour-compression cycle for refrigerating system

(Bolaji *et al.*, 2019)

Different refrigerants have been used for refrigeration depending on the desired output, however, the most commonly method used to study the behaviour of refrigerants is p-h (pressure-ethalpy) chart which is a plot of several horizontal and vertical lines. A few of the lines are plotted as shown in Figure 2.15.

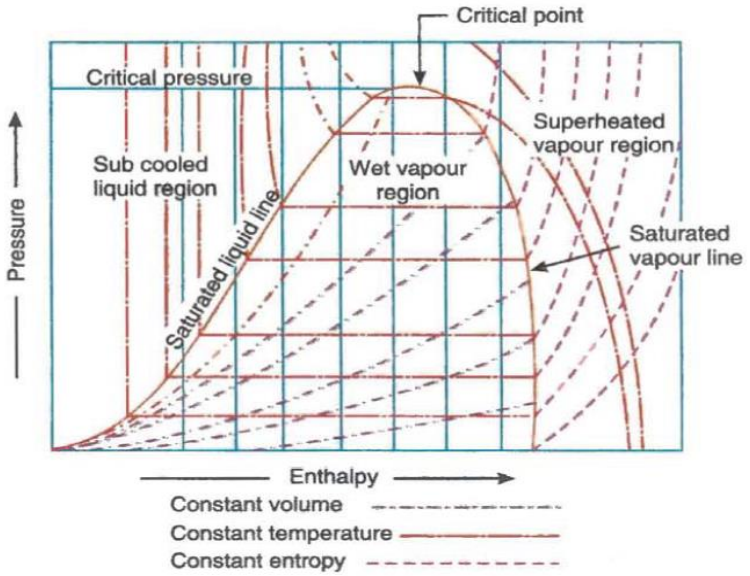

Figure 2.15: Pressure-Enthalpy chart

(Khurmi and Gupta, 2016)

The horizontal lines also known as total heat represents enthalpy while the vertical lines represent pressure; the critical point being the point at which the saturated liquid and saturated vapour lines meet while the region that falls within the two lines is the wet vapour region. The region at the left of saturated liquid line is the sub-cooled liquid region while the region at the right of the saturated vapour line is the superheated vapour region. In theory, the vapour-compression cycle for dry saturated vapour after compression has been explained in (Khurmi and Gupta, 2016) with Figure 2.17a,b which are the temperature-enthropy (T-s) and pressure-enthalpy (p-h) as follows:

At point 1, the vapour refrigerant is compressed at low temperature and pressure T_1 and P_1 as shown by the line 1-2 on the T-s chart and curve 1-2 on the p-h chart respectively; at this point the temperature, pressure and entropy of the liquid refrigerant are represented by T_1, P_1 and s_1. After compression, the temperature and pressure are then

increased from T_1 to T_2 and from P_1 and P_2, while h_1 and h_2 are the enthalpies of the vapour refrigerant at temperature T_1 (entry of the compressor) and temperature T_2 (at discharge from the compressor). The vapour refrigerant at high temperature and pressure moves to the condenser where it is condensed at constant temperature and pressure T_2 and P_2 as shown by the line 2-3 on the T-s and p-h charts (Figure 2.16).

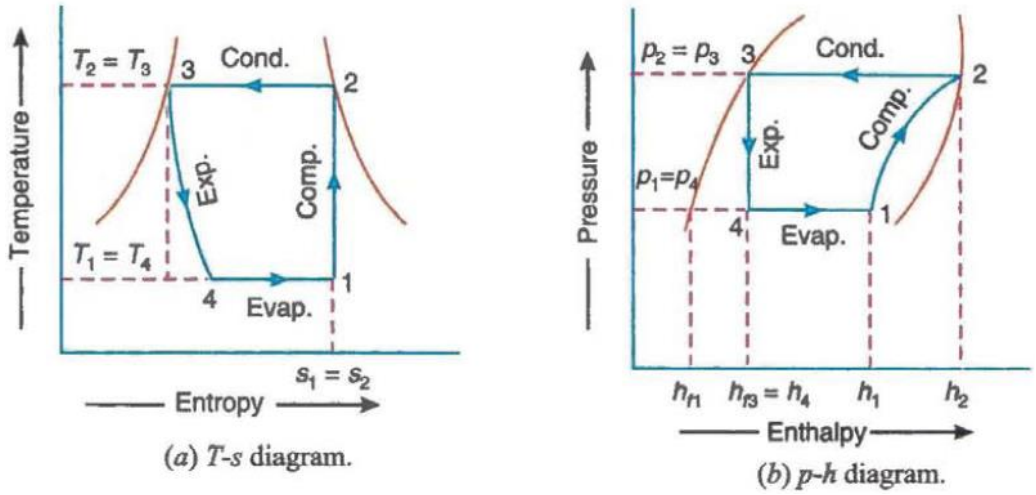

Figure 2.16: Representation of vapour-compression cycle with dry saturated vapour after compression

(Khurmi and Gupta, 2016)

In the condenser, the vapour refrigerant therefore changes to liquid refrigerant and it gives latent heat to the surrounding condensing medium while passing through the condenser. In the expansion valve throttling process occurs and the liquid refrigerant at temperature $T_2 = T_3$ and pressure $P_2 = P_3$ is expanded to a low temperature $T_4 = T_1$ and low pressure $P_4 = P_1$. The expansion process is shown by the curve 3-4 and line 3-4 on the T-s and p-h diagrams. However, h_{f3} is the heat at temperature T_3 which corresponds to the enthalpy of the liquid refrigerant leaving the condenser. In line 4-1 on the T-s and p-h diagrams, the liquid-vapour mixture of the refrigerant at constant temperature $T_4 = T_1$ and constant pressure $P_4 = P_1$ becomes evaporated and changes to vapour; and the

process of vapourization continues to point 1 on the charts to start another cycle (Figure 2.16).

2.8.3 Review of related literature on chillers

Cooling and heating are useful processes often required in various areas such as buildings, hotels, malls, hospitals, restaurants, automobile to mention a few. Cooling has significantly been achieved by refrigeration in domestic, commercial and industrial activities which include its use in the preservation of foods, beverages and other activities that require refrigeration. One of the most important components of chillers or refrigerators is the refrigerant used for cooling. An ideal refrigerant has been mentioned to possess properties such as low boiling and freezing point, high critical temperature and pressure, low cost , non-toxic, non-corrosive to metals and ozone friendly (Khurmi and Gupta, 2016). These properties are not limited to the mentioned ones but among them, priority has been given to the encouragement of the use of refrigerants that are ozone friendly. Primary refrigerants are classified as halo-carbon or organic, azeotrope, inorganic and hydrocarbon refrigerants.

Organic refrigerants have been the most commonly mentioned and the American Society of Heating, Refrigeration and Air-conditioning Engineers (ASHRAE 2013) identified 42 halo-carbon compound as refrigerants, 15 of which have been the most commonly mentioned in the literature. These are R-11, R-12, R-13, R-14, R-21, R-22, R-30, R-40, R-100, R-113, R-114, R-115, R-123, R-124, R-134a and R-152a; with each of them having their chemical name and formula as detailed in (Khurmi and Gupta, 2016). However, it has been argued that some of these refrigerants are ozone depletion and efforts have been made to replace them by comparing their performance with other refrigerants. Possible alternative refrigerants that have been mentioned include hydrocarbons (HCs) such as R290, R1270 and their mixtures (R432A, R433A);

hydroflurocarbons (HFCs) R401A, R410A and R407C (Ramu *et al.* 2014). For example, (Jain *et al.* 2011) carried out comparative analysis of vapour compression refrigeration system using R-22 refrigerant and environmentally-friendly hydroflurocarbon (HFC) refrigerants:R-134a, R-410A, R407C and M30 with the aim of proposing replacement for R-22 refrigerant. Hadya (2016) simulated vapour compression refrigeration system using different refrigerants; R-22, R410A and R-32. The COPs of the system were found to be 2.33, 3.36 and 3.63 for R-22, R410A and R-32 refrigerants respectively. However, only results obtained numerically were presented in the investigation (Hadya, 2016). The performance of vapour compression system could also be evaluated by mixing two hydrocarbon refrigerants in comparison with hydroflurocarbon refrigerant. One of such cases include the work of (Saibhargav *et al.,* 2019) where the performance of R134a was compared with that of the mixture of R290 and R600a in a 30 litre capacity vapour compression water chiller. Better performance was revealed using the mixture of R290 and R600a in terms of evaporating and condensing temperature; and power consumption compared to the usage of R134a.

However, care must be taken regarding the activity of mixed refrigerants on the performance of compressors, as replacing the commonly used refrigerants with mixed ones may be a significant challenge due to the need to redesign compressors (Bolaji *et al*. 2019) The performance evaluation of vapour compression chiller was carried out in a 400 seat auditorium using R290 refrigerant (Fuadi *et al.,* 2019). The results revealed a maximum COP of 4.27 with a cooling effect of approximately 125.93 kW and a compressor output of 30.06 kW. Nanofluid related refrigerant have also been considered for use in refrigeration due to the quest for sustainability. In (Adelekan *et al.,* 2019), 15 nm TiO_2-R600a nano-refrigerant was used to investigate the performance of vapour compression refrigerator. It was revealed that the nano based refrigerant performed

better in terms of refrigeration effect and COP of the system compared to pure R600a refrigerant. Regarding R-22 refrigerant, at this juncture, it must be mentioned that there is no specific conclusion in the literature suggesting that R-22 refrigerant should be replaced completely in current refrigeration designs and due to easy availability low cost compared to other imported refrigerants; and good thermodynamic and thermo-physical properties (Ramu *et al.*, 2014). R22 is still most widely used in vapour compression refrigeration. However, its usage has been limited to the year 2030 for developed countries and year 2040 for developing countries (Fuadi *et al.*, 2019). This is why studies such as Tian *et al.* (2014) and Wu *et al.*, (2012) have carried out experiments using R290 refrigerant, which in the future may also be discouraged due to its flammability (Wu *et al.*, 2012).

Chillers have been developed for several purposes. Ayres, (2013) developed a 12 Kw air-cooled water chiller with a coefficient of performance of approximately 2.2 and for cooling water from a temperature of 20 ^{o}C to a temperature of 10 ^{o}C using R-134a refrigerant. Although several assumptions were made in the design calculations and these affected the overall performance of the chiller. Coefficient of performance (COP) of a chiller or refrigerator is the amount of the amount of heat produced by the refrigerator to the amount of work done on the refrigerant; however, the COP of refrigerating unit is usually 2 (Khurmi and Gupta, 2016). Another typical example of a chiller is the absorption type chiller which works with different principle of operation compared to the compression refrigerators. Both are refrigerating systems but the major difference between them is that in the compression refrigerator, the refrigerant changes from gas to liquid after compression has taken place while in the absorption chiller, the gas changes to liquid using heat energy. In order words, absorption chillers are heat driven refrigerators that use liquid refrigerant heat source to achieve cooling. The

external heat that serves as the power source could be in the form of steam, natural gas and waste heat; with the heat being transferred in form of thermal energy via the heat source to the absorbent fluid and refrigerant (Ugwu, 2012). Absorption chillers can be categorized as one of the alternatives to compression refrigerators and they work using the absorption principle without compressors which are replaced with by an absorber, a generator and pressure reducing valve which in essence makes them silent while in operation (Khurmi and Gupta, 2016). The working principle of absorption chiller is shown in Figure 2.18, with the presence of heat source and absorber showing the major difference between absorber chillers and vapour-compression refrigeration cycle. Mechanical heat pumps using absorption principle have been mentioned to contribute significantly to the in ozone layer depletion and climate change (Demir *et al.*, 2008). Other advantages of absorption heat pumps less maintenance requirement and their ability operate using energy sources such as waste heat and solar (Demir *et al.*, 2008). However, their lower coefficient of performance and the cost involved in developing absorption chillers have been mentioned as their limitations (Demir *et al.*, 2008; Ugwu, 2012). It was also mentioned that the currently available absorption refrigeration systems are expensive with respect to the capital expenditure (CAPEX) and operating expenses (OPEX) (Ayou and Coronas, 2020).

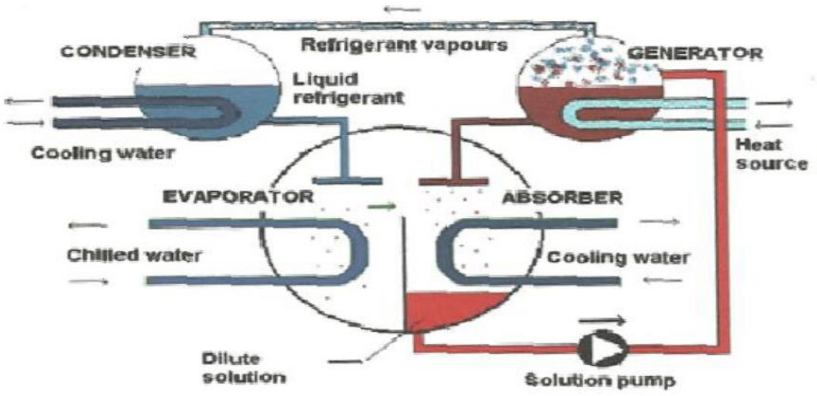

Figure 2.17: Working principle of an absorption chiller

(Ugwu, 2012)

An absorption chiller was developed by (Ugwu, 2012) using locally sourced materials. The materials used for the fabrication include condenser, heat sink, evaporation, wood and ammonium/water absorber refrigerant. Both gas and electric arc welding was used for fabrication and the dimension of the casing was 45.5 cm length, 50 cm height and 30 cm breadth while the number of turns of the condenser was estimated to six turns as recommended in (Khurmi and Gupta, 2016). The system was powered by 250 volts generator and the coefficient of performance (COP) was determined to be 1.21 while the refrigeration effect was 1457.99 kJ. Since most refrigerators are electrically powered, an alternative eco-friendly and renewable source of energy may be needed for operation of refrigerators and chillers in situations where there is inadequate power supply as experienced in Nigeria, compared to the use of generator as adopted in (Ugwu, 2012). For example, solar powered cooling refrigeration would help to reduce the consumption of fossil fuels as well as significant reduction in carbon emission (Ayou and Coronas, 2020). Also, most seawater and temperature related corrosion experiments are carried out without interruption of the system if results that are similar to structures operating in-situ are desired. It should therefore be mentioned that corrosion rigs must be designed putting into consideration the source of energy to operate the system.

Several modifications to vapour compression refrigeration system have been carried out to either optimize the performance of the system of investigate the refrigeration capacity by changing the types of refrigerants used. For example, (Sutthivirode and Thongtip, 2020) carried out experimental analysis of vapour-compression water chiller with the performance being influenced by different expansion devices which are thermostatic expansion valve, needle valve and capillary tube, in order to investigate the system refrigeration performances such as COP, cooling temperature and load; and electricity

consumption in a designed and fabricated 2000 W chiller. The refrigerant used was R134a and the cooling capacity of the evaporator was 3500 W while the heat transfer capacity of the condenser was 7000 W. It was found that the highest COP was obtained with the needle valve followed thermostatic expansion valve while the least COP was achieved with the use of capillary tube due to its inability to control the mass flow rate of the refrigerant compared to the other two expansion devices. This implies that expansion devices have significant effect on performance of vapour compression refrigeration system with respect to compressor, condenser and evaporator as mentioned in (Choi and Kim, 2020). As such, the reason was attributed to the dominant nature of expansion devices in controlling the low and high pressure associated with the refrigeration cycle as well as the flow rate of the refrigerant.

It was also mentioned that characteristic effects of different devices could influence the performance of the system during throttling process (Bagarella *et al.,* 2013 and Liu *et al.,* 2018). The significant effect of different expansion devices vapour compression refrigeration was also revealed in the investigation carried out by (Liu *et al.,* 2018). As part of food preservation property of refrigeration systems, a 20 kg capacity vapour compression refrigeration system equipped with temperature control device was developed for the preservation of vegetables using R134a refrigerant (Mogaji, 2019). The refrigeration system improved the shelf life of the vegetables used for investigation by 14 days with the cabinet temperature maintained at 3.64 ^{o}C at an ambient temperature of 26.89 ^{o}C.

However, most of the vapour compression chillers that have been mentioned in the literature are those used for cooling in electronic devices (Siricharoenpanich *et al.,* 2019; Jajja *et al.,* 2014) water chillers for cold drinks (Du-Plessis *et al.,* 2015) (Mohammadi and McGowan, 2018) hydroponics farms, and water chillers with using

different expansion devices under transient conditions (Sutthivirode and Thongtip, 2020). The recent use of chillers for corrosion fatigue experiment was reported in (Adedipe, 2015); however, the chiller that was used for the corrosion rig design was an imported type which is also used in aquariums. Hence, the need to develop cost effective chiller for corrosion experiment using locally sourced materials.

The performance evaluation 5 ton water chiller with R404A refrigerant and with two different configurations was carried out by (Arya and Chavda, 2014). The first configuration was scroll compressor and plate heat evaporator while the second one was with scroll compressor; and shell and tube evaporator. It was found that the former gave better results in terms of the system performance than the latter. Thu *et al.,* (2017) investigated the performance of mechanical vapour compression chiller at elevated chilled water outlet temperature range of 7 to 17 ^{o}C and at coolant temperature range of 28 to 32 ^{o}C. An increase of 3.5 % in the COP of the chiller was observed at every increase of the chilled water temperature, while the cooling capacity of the chiller increased by 4 %. It was also found that at a water outlet temperature of 17 ^{o}C, the COP and the cooling capacity of the chiller were between 37-40 ^{o}C and 40-45 ^{o}C respectively. Another design of vapour compression refrigeration system is the one developed by (Fong *et al.,* 2011) where solar-electric compression system was equipped with an ejector assisted vapour compression chiller as shown in Figure 2.18.

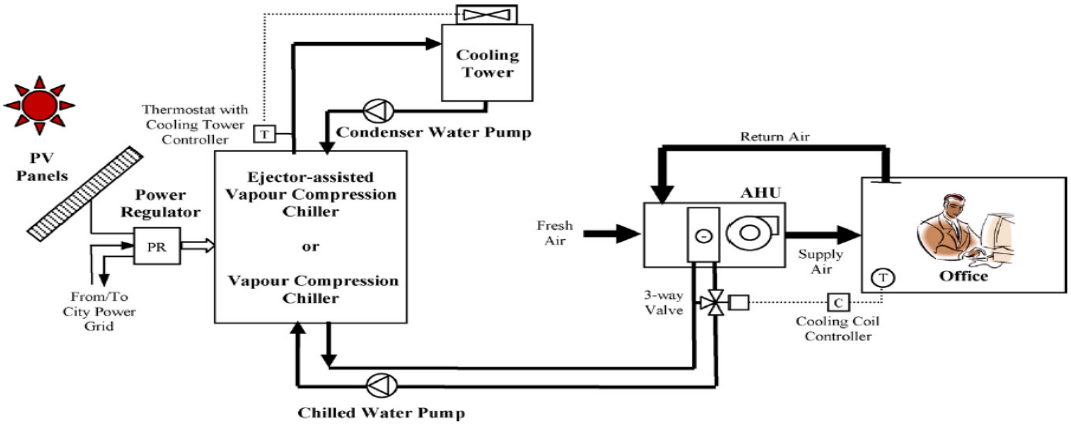

Figure 2.18: Solar powered ejector assisted compression refrigeration system (Fong *et al.*, 2011)

The function of ejector assisted design was to raise the action of the gas refrigerant in the evaporator thereby reducing the power input of the compressor as well as decreasing the enthalpy being dissipated by the capillary tube (expansion valve). Three refrigerants R22, R134a and R410A were used to investigate the annual energy performance of the system. It was found that R134a had the best performance in terms of energy saving followed by R22 while R410A revealed the least energy saving. The work reported by (Fong *et al.*, 2011) suggests that more than one refrigerant could be used to investigate the performance of refrigeration systems with minor modifications to the initial design. An example of such experiments include the one carried out by (Oyedepo *et al.*, 2016) where the performance of domestic refrigerator designed for R12 refrigerant was investigated with refrigerant R600a and by changing the capillary tube length. The investigation revealed the highest cooling capacity of 9.18 % using R600a and with lowest power consumption using the 1.5 m capillary tube length which summarily showed that R600a performed better than R12. Recently, (Madriya *et al.*, 2019) investigated the performance of R600a using different capillary tube length: 1.0, 1.15, 1.30 and 1.45 m on a refrigerator that was designed for R134a. The optimum capillary tube length of 1.30 m revealed an increase in COP and cooling capacity of R600a by 45

% and 4.2 % respectively while power consumption of the refrigerator reduced by 25 % compared to the performance using R134a.

CHAPTER THREE

MATERIALS AND METHODS

3.1 Materials

The material that was used for investigation was a 600 x 150 x 20.8 mm API X70 steel plate/pipe weldment. The welding of the plate was carried out using the manual metal arc welding facility located at SCC Nig. Ltd. at Ushafa, Bwari, FCT Abuja. The remaining materials and equipment that were used for the research include the following:

i. Welded X70 pipeline steel;
ii. Manual metal arc welding machine/facility;
iii. A designed and developed corrosion rig;
iv. Natural
v. Chiller;
vi. Thermometers;
vii. Pumps;
viii. pH meter;
ix. Digital microscopes;
x. Tensile test machine;
xi. Izod impact test machine;
xii. Vickers hardness machine
xiii. Grinding and Polishing machine
xiv. Scanning electron microscope (SEM)
xv. X-ray fluorescence and X-Ray diffraction machine

3.2 Methods

3.2.1 API X70 steel material characterization and spectroscopic analysis

In order to establish the conformity of the chemical composition of the steel plate with the chemical analysis that was spelt out in the steel manufacturers certificate, the chemical analysis was carried out at the Oshogbo Machine Tools, Oshogbo Osun state. A cut out of dimension 40 x 30.5 x 20.8 mm was extracted from the steel plate for the chemical analysis. Spectroscopic analysis was conducted on the material in order to reveal the steel material elements and their compositions. The outcome of the spectroscopic analysis conducted on the material showing locations of sparks can be seen in Plate I.

Plate I: Spectroscopic analysis

3.2.2 Microstructure examination of test sample

A cut out of dimension 40 x 30.5 x 20.8 mm was extracted from the steel plate for microstructural examination. The sample was polished using emery papers of grade 200 until a mirror surface was achieved. The surface of the sample was washed with water

and was later dried. The macro-examination was then carried out using optical microscope equipped with an in-built camera and computer facilities belonging to Oshogbo machine tools, Osun State and Obafemi Awolowo University, Osun State. Magnifications taken at 400, 200 and 100 respectively. Prior to the analysis, the sample was prepared by grinding using the South bay Technology Grinder /polisher Machine, model 900 shown in Plate ii accompanied with silicon carbide papers of grades 220, 320, 400 and 600. The sample was then washed with running water to clear the debris arising from the silicon carbide paper. A universal polishing machine was used with polishing cloth and final polishing was done to obtain a mirror like surface using polishing cloth applied with 0.5 μm silicon carbide. The sample was then washed and dried. In order to reveal the microstructure of the sample etching was carried out using 2 % Nital. The sample was washed, dried and was subsequently examined using the Princeton, US Microscope (Serial no 0524011) equipped with inbuilt camera in Plate II and Plate III indicated Microscope with camera.

Plate II: Grinder /polisher machine model 900 (South bay Technology)

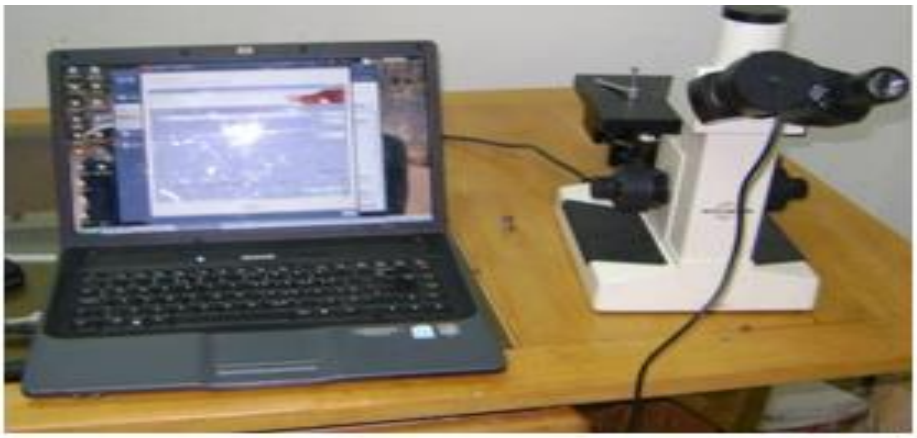

Plate III: Microscope with camera (Serial no 0524011, Maker:Princeton, US)

3.2.3 Weld material and sample preparation

After establishing the chemical composition of the material, the welding was conducted using the welding facility located at SCC Abuja. Prior to edge and welding preparation, the 20 mm thick plate was cleaned to avoid any impurities that may be trapped in the weld area. A double V butt welded preparation was adopted during the welding process. A groove angle of 60º, root face of 6 mm and root spacing of 0.3 mm was used. The groove designed for the plate edge preparation is shown in Figure 3.1.

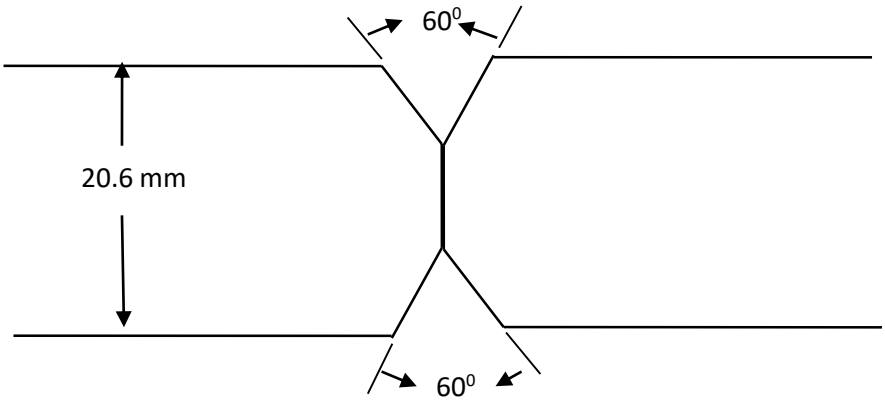

Figure 3.1: Groove designed for the edge preparation

The manual metal arc (MMA) welding technique was used coupled with flat welding positions (1G) during welding. The electrode used was designated E7018), with 4mm diameter wire. It was ensured that the chemical composition of the filler material was similar to that of the parent material.

3.2.4 Extraction of test samples

Tensile and compression samples were extracted from the weld and parent materials. Samples for impact and hardness tests were also extracted at the relevant areas of the plate (weld, parent and HAZ). It was difficult to extract samples for tensile and compression test due to the limitation of the machine to accommodate size of the specimens that would be required for testing considering the size of the heat affected zone. Prior to the extraction, the weld was characterized in order to reveal the heat affected zone. A small sized sample was cut from the weld area and was machined to a size that accommodates the sample holder; the sample was polished and etched using 2 % Nital solution. After the etching, the sample was washed with water and the weld areas was revealed as shown in Plate IV. The HAZ was measured to be averagely 2.5 mm by width.

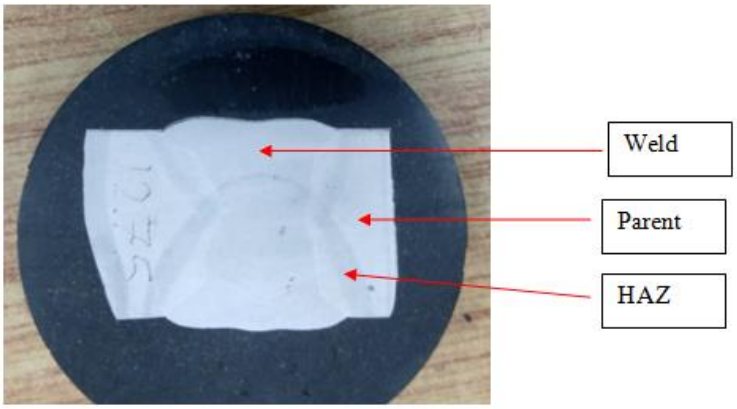

Plate IV: Polished and etched sample showing weld, parent and HAZ

The impact test samples were V-notched and the notches were prepared by notch-making machine at SCC Abuja to achieve a notch base radius of 0.25 mm. The notches of the samples for impact tests were therefore machined to align with the parent, weld and HAZ. A similar procedure was done for sample used for hardness. A typical sample used to carry out the hardness test is shown in Figure 3.2.

3.2.5 Tensile test

Tensile tests were carried out according to the ASTM E8 (ASTM E8 2013). Tensile tests for all samples was carried out at SCC Nig Ltd Abuja using UNITED type universal tensile testing machine with number S/N 0405536 as shown in Plate IV. While Plate V shows some of the tensile test specimens that were tested.

Plate IV: Tensile testing machine (UNITED type)

: 

Plate V: Tensile test specimens

All the tests were carried out according to ASTM E8 (ASTM E8 2013). A total of twenty tensile samples were tested. For air test, ten parent and weld samples were tested and ten parent and weld samples that were immersed in seawater were tested after the seawater corrosion test. Before the tests were carried out, the total lengths of the tensile samples were measured to be 320 mm using linear caliper. The samples were marked for identification and were gripped in the jaws of the tensile testing machine i.e. the upper and the lower jaws one after the other. The samples were then subjected to a gradually increasing tensile load and reading was taken both at yield and maximum load until fracture occurred. The results were plotted automatically by the computer that was attached to the machine. Readings were also taken during the tests.

3.2. 6 Impact test

The impact tests were carried out according to ASTM E23 (ASTM E 23 2014) using the impact test machine shown in plate vi which is located in SCC Abuja. For each test, the specimen was mounted on the testing area of the impact testing machine and the striking pendulum was released to fracture the specimen through the impact load. The corresponding energy that absorbed by the specimen at fracture was recorded from a

gauge attached to the machine. The process was repeated in all the specimens (parent, weld and HAZ specimens) tested.

Plate V: Impact testing machine

3.2. 7 Compression test

Compression test was carried out at the department of material science and engineering, Obafemi Awolowo University, Ile Ife Nigeria. The compression test was carried out according to ASTM E8 using computerized Instron Testing Machine (model 3369) shown in plate vi. The tests were carried out at room temperature with a strain/ loading rate of 5 mm/mn. Load displacement plots were obtained on an X – Y recorder and the compression strengths were determined from the load displacement diagrams.

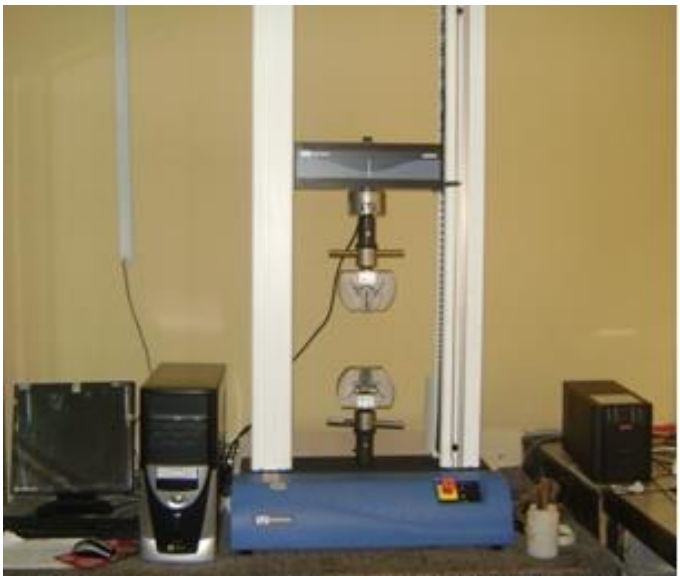

Plate VII: Universal instron machine (model 3369)

3.2. 8 Hardness test

Hardness tests were also carried out according to ASTM E384 (E384 2012) and API 5L/ISO3183 FIG J1 using Vickers hardness tester at SCC Nig. Ltd. Abuja. The hardness test was carried out through the indenter at a load 190 g. A total of 33 hardness values were measured on the weld specimen used and the interval of testing of one point to another was 2 seconds.

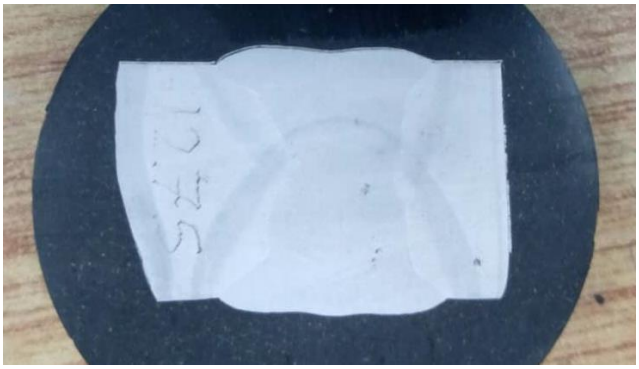

Plate VIII: Hardness test sample

A total of 6 points were measured on parent material while 18 points were measured on the HAZ and a total of 9 points were measured on the weld. The specimen that was used

for hardness test was prepared by polishing and etching thereby revealing the parent, weld and HAZ of the material as shown in plate viii.

3.2.9 SEM analysis

The SEM analysis was carried out using the ZEISS SEM machine available at Obafemi Awolowo University (OAU), Ile Ife Nigeria. Before the analysis was carried out, it was ensured that the cracked samples were cleaned with spirit. The samples were arranged in the machine as shown in plate IX.

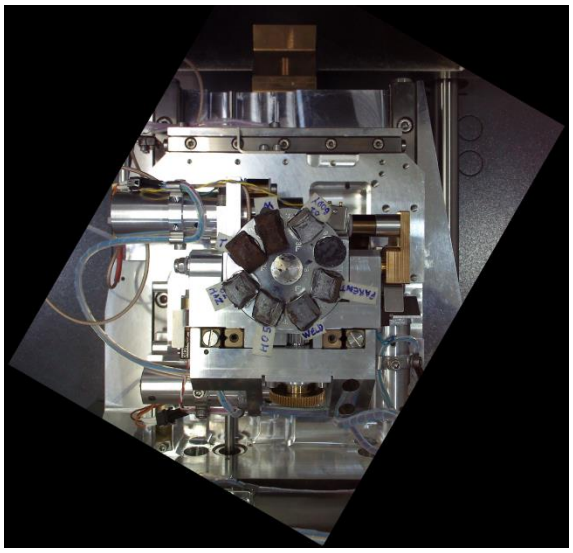

Plate IX: Scanning electron microscope (SEM) analysis

The analysis was carried out on only selected areas of the surfaces of the samples and were analysed using 100X, 250X, 500X and 750X magnifications respectively. Several dimensions of the selected surfaces ranging from 30 µ to 300 µ were considered during the analyses.

3.2. 10 X-ray diffraction (XRD) and X-ray fluorescence (XRF) analyses

The XRD analysis was carried out using Miniflex XRD Rigadu machine at OAU, Ile Ife. The XRD was operated using the following instrumental setting conditions: Nickel

filtered Fek and radiation, recording/scanning rate of 1’ 20cm/min, time of constant 4, range of 4 x 10 C.P.S and Voltage of 28 kV /12 mH. In order characterize the elements of the steel sample, the XRF analysis was carried out using Phillips PW-1800 XRD machine. Both XRD and XRF analyses were carried out at OAU, Ile Ife. The prepared test sample was loaded in the spectrometer test chamber and generator current of 20 mA and voltage of 40 kV were used to excite the X-ray on the test sample. The corresponding spectrum generated from the sample was then analysed.

3.3 Development of Corrosion Rig

The developed corrosion rig comprises of components ranging from the water reservoir, chiller and test chamber all connected in one unit. The components were selected based on the design factors which include types of material and availability, performance requirement. The components were designed as follows:

3.3.1 Materials for corrosion rig

The corrosion rig used for experimental investigation in this work was developed in order to represent in the laboratory a similar nature of the environment that pipelines installed in seawater experience. A similar seawater environment was prepared and circulated through the specimens. This section describes the design consideration, material used, design analysis and calculations and the fabrication procedure. The materials used for the fabrication includes the mild steel sheet, stainless steel sheet, angle iron, rivets, bolts, two plastic buckets, 1 inch and ½ inch flexible pipes, transparent Perspex chamber, two aphacool pumps, compressor coupled with fan, evaporator, condenser, expansion valve, thermostat and electrical control unit equipped with temperature display. The thermostat was used to monitor the temperature at the reservoir. Mild steel sheet and angle iron were used to construct the chiller frame,

reservoir stand and the Perspex chamber stand. Stainless steel was used fabricate the chilling unit, rivet pins and bolts were used for the assembly of some of the parts of the chillers while the other parts were welded. The two plastic buckets were used to fabricate the reservoir while the flexible pipes were used to move the water through the pumps from the reservoir to the chiller to the chamber and back to the reservoir. The pumps assisted in pumping and circulating the water through the units.

3.3.2 Design consideration

The following factors were considered for the chiller corrosion rig design:

i. Availability of the materials
ii. Cost of fabrication in comparison to in-situ testing
iii. Suitability of the material for the operating condition
iv. Seawater temperature
v. Volume of the water required in the chamber
vi. Coefficient of performance of the chiller

3.3.3 Design analysis

One of the important design consideration was based on the target temperature of seawater that will be achieved at the test chamber in order to mimic the typical (Lagos) Nigeria seawater temperature which has been reported to be averagely 28 ^{o}C. This informed that temperature to be achieved at the evaporator and subsequently at the test chamber.

3.4 Chiller design

Since the chiller has almost similar principle of operating to the refrigerator, the vapour-compression refrigeration cycle was adopted in the design. However, the most notable

difference between refrigerating systems and the chiller used for this research is that the water is passed after the temperature has been reduced to the chamber containing the specimen, unlike in refrigerating units where the chilled water remained in the cabinet. Another significant difference is that the chilling chamber was fabricated with stainless steel in order to avoid corrosion arising from the seawater that was used for experimental investigation. In the design of the chiller, vapour-compression cycle was considered as shown in the temperature-entropy (T-s) and pressure-enthalpy (p-h) diagrams in Figure 3.3. The process has been described in chapter 2 but the associated parameters are outlined in this chapter.

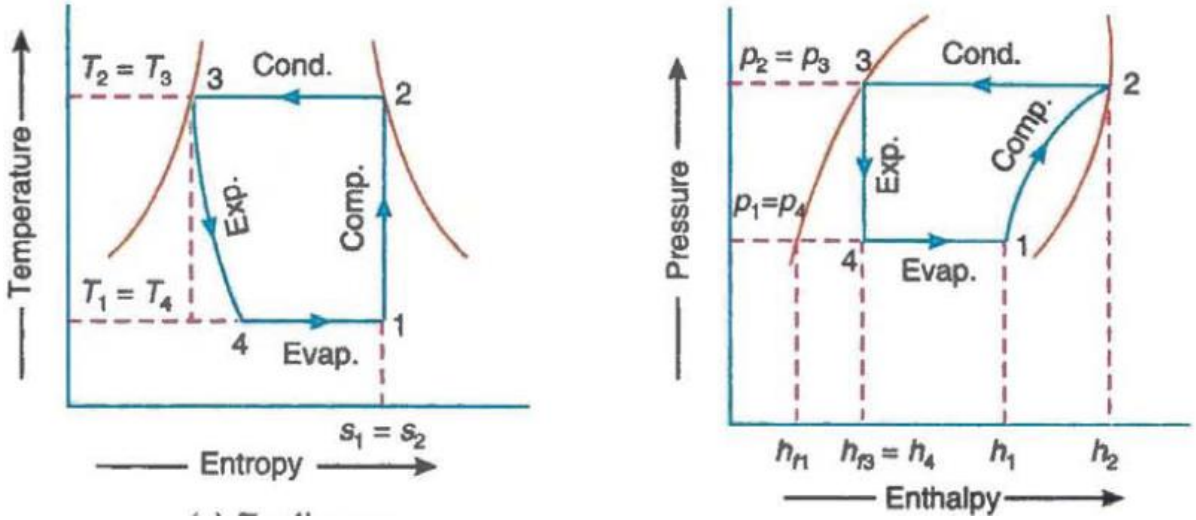

(a) (b)

Figure 3.3: Vapour compression cycle with dry saturated vapour after compression for (a) T-s diagram, (b) p-h diagram (Ugwu, 2012)

At the initial stage (point 1), the vapour refrigerant is associated with low temperature and pressure and represented by $T1$ $P1$and $S1$ $h1$

Where:

$T1$ = Temperature of the vapour refrigerant (K),

$P1$= Pressure of the vapour refrigerant (bar),

$S1$=Entropy of the vapour refrigerant (kJ / kgK),

$h1$= Enthalpy of vapour refrigerant at temperature $T1$ (entrance of the compressor) (kJ / kg)

At point 2, during compression, the vapour is compressed isentropically; the pressure and temperature and pressure are increased to $T2$ and $P2$ as shown in line 1-2 and curve 1-2 (Figure 3.3a and b). The corresponding workdone during the isentropic compression per kg of the refrigerant is therefore given by (Khurmi and Gupta, 2016) as:

$$w = h_2 - h_1 \quad (3.1)$$

Where:

$T2$= Temperature of the vapour refrigerant at the discharge of the compressor (K)

$P2$= Pressure of the vapour refrigerant at the discharge of the compressor (bar)

$h2$= Enthalpy of vapour refrigerant at temperature T_2 (discharge of the compressor) (kJ / kg),

During the condensation stage (line 2-3), the vapour refrigerant at high temperature and pressure is passed through the condenser where it is completely condensed at constant pressure p_2 and temperature $T2$ At this point the vapour refrigerant changes to liquid and remains at the constant pressure and temperature $P3$ and $T3$ at point 3. Heat h_{f3} is released into the surrounding medium during condensation.

Where:

$P3$= Pressure of the liquid refrigerant at the discharge of the condenser (bar),

$T3$= Temperature of the liquid refrigerant at the discharge of the condenser (K),

$h3$= Enthalpy (latent heat) of the liquid refrigerant leaving the condenser (kJ/kg)

During expansion process, the liquid refrigerant at $p_3 = p_2$ and temperature $T3 = T2$ is expanded by the expansion valve to a lower pressure $P4 = P1$ and temperature $T4 = T1$. This is shown by line 3-4 and curve 3-4 in Figure 3.3.

Where:

$P4$= Pressure of the liquid refrigerant at the discharge of the expansion valve (bar),

$T4$= Temperature of the liquid refrigerant at the discharge of the expansion valve (K)

During the vapourisation process at point 4, the liquid-vapour mixture refrigerant at pressure $P4 = P1$ and temperature $T4 = T1$ is evaporated and changed to vapour up to point 1 in order to begin another stage. The vapourisation stage is represented by lines 4-1 in Figure 3.3.

The heat that is absorbed by the refrigerant is called refrigerating effect RE and is expressed as:

$$R_E = h_1 - h_4 = h_1 - h_{f3} \quad (3.2)$$

Equation 3.2 implies that $h4 = hf3$

Where $h4$ = Enthalpy of refrigerant at the discharge of the expansion valve (kJ/kg)

RE = Refrigerating effect (kJ/kg)

For a vapour compression cycle, the coefficient of performance (C.O.P) is determined by Equation 3.3 as:

$$C.O.P = \frac{Refrigerating\ effect}{Work\ done} = \frac{R_E}{w} \quad (3.3)$$

Equation 3.3 can be expressed in terms of enthalpies as

$$C.O.P = \frac{h_1 - h_4}{h_2 - h_1} = \frac{h_1 - h_{f3}}{h_2 - h_1} \quad (3.4)$$

3.4.1 Properties of refrigerant R-22

The refrigerant R-22 belongs to the class of halo- carbon refrigerant and is used in air conditioning and refrigerating units. It is not toxic, not corrosive and not flammable. The chemical name of R-22 is Monochloro-trifluoro-methane while the chemical formula is $CHClF_2$. It was used for this research work. Although R-134 has been proven to be the best in terms of energy saving, availability and cost is major hinderance to its usage hence, R-22 was preferred for use in this research work. Generally, in refrigeration, the operating temperature of R-22 is based on evaporating temperature of -15 ^oC and condensing temperature of 30 ^oC. However, refrigerant R-22 has the following properties: boiling point is -41 ^oC at atmospheric pressure, latent heat and evaporator pressure at a temperature of -15 ^oC are 216.5 kJ / kg and 1.92 bar while the normal head pressure at a temperature of 30 ^oC is 10.88 bar, the freezing temperature is -160 ^oC; and the evaporator pressure at -15 ^oC and condenser pressure at 30 ^oC are 2.9670 bar and 12.0340 bar respectively. The critical temperature which the highest temperature at which the refrigerant R-22 can be condensed into a liquid irrespective of the higher pressure is 96 ^oC while the corresponding critical pressure is 49.38 bar. The refrigerating effect of R-22 operating from a temperature of -15 ^oC to a temperature of

30 ^{o}C is 161.5 kJ/kg while the latent heat of vapourisation at a temperature of -15 ^{o}C is 218.1 kJ/kg.

3.4.2 Design of chiller cabinet

The chiller cabinet contains the frame, chilling unit, compressor, condenser, expansion valve, evaporator and the electrical control; all combined together as a unit. Some of the important parts/components of the chiller were designed as follows:

a. Area of the chiller cabinet

The cabinet casing or housing was determined by considering the size of the chilling unit, space for the compressor, the space for the condenser and the other faces of the cabinet that are closed.

The area of the cabinet was determined according to the relationship in equation 3.5 (Ugwu 2012)

$$A_c = 2(LW) + 2(LH) + 2(WH) \quad (3.5)$$

Where A_c is the area of the cabinet (mm^2),

L is length of cabinet (mm)

H is height of cabinet (mm)

W is width of cabinet (mm)

b. Volume of the cabinet

The thickness that was considered for the cabinet was used based on the thickness of the frame that supports the six sides/faces of the cabinet. The thickness of the frame was 25.40 mm. Therefore, assuming that the thickness has been encompassed as part of the

dimensions for height, length and width of the cabinet, the volume of the cabinet can be mathematically expressed as:

$$V_c = L\ x\ W\ x\ H \tag{3.6}$$

c. Area of the chilling chamber

The chilling chamber was a stainless steel fabricated as two concentric cylinders. The water is chilled at the compact space between the two cylinders while the evaporator was coiled round the hollow surface of the inner cylinder to facilitate the cooling. The total surface area of the chiller chamber was therefore determined by equation 3.7

$$A_{CC} = 2\pi\left({R_o}^2 - {r_i}^2\right) + (2\pi R_o l_c + 2\pi r_i l_c) \tag{3.7}$$

By factorization, Equation 3.7 becomes:

$$A_{CC} = 2\pi(R_o + r_i)(R_o - r_i + l_c) \tag{3.8}$$

Where:

A_{cc} is the total surface area of the chilling chamber (mm^2),

R_o is the radius of the outer surface of the chilling chamber (mm),

r_i is the radius of the inner surface of the chilling chamber (mm),

l_c is the length of the cylinder (mm).

d. Volume of the chilling chamber

The volume of the chilling chamber was determined by the relationship

$$V = \pi r^2 h \tag{3.9}$$

However, considering hollow cylindrical shape, the volume of the chilling chamber can be re-written as:

$$V_C = \pi l_c\left({R_o}^2 + {r_i}^2\right) \quad (3.10)$$

Where V_c is volume of the chilling chamber (mm^3).

e. Mass flow rate

The mass flow rate of the system was determined using the relationship in (Ugwu 2012) as:

$$M = \frac{Refrigeration\ capacity\ of\ the\ system}{Refrigerating\ effect} = \frac{Volume\ of\ the\ chilling\ cabinet}{Refrigerating\ effect} \quad (3.11)$$

Equation 3.12 can be expressed mathematically as:

$$M = \frac{V_c}{R_E} \quad (3.12)$$

Where M is mass flow rate ($kJ^{-1}kgm^3$)

f. Capacity of the condenser

The capacity of the condenser was determined by (Ugwu, 2012)

$$C_c = M(h_2 - h_3) \quad (3.13)$$

Where C_c is the capacity of the condenser TR (Tonnes of refrigeration)

g. Capacity of the evaporator

The evaporator capacity was determined by (Ugwu, 2012):

$$C_e = M(h_1 - h_4) \quad (3.14)$$

Where C_e is evaporator capacity (kJ)

3.4.3 Design of corrosion rig reservoir

Since operating environment of the corrosion rig is seawater; therefore, the reservoir was fabricated using plastic bucket in order to avoid corrosion at the reservoir.

a. Area of the reservoir

The area of the plastic reservoir can be determined using the area of a cylinder and this is expressed as:

$$A_r = 2\pi R_r l_r \tag{3.15}$$

Where A_r is the area of the reservoir (mm^2),

R_r is the radius of the reservoir (mm),

l_r is the height of the reservoir (mm).

b. Volume of the reservoir

The volume of the reservoir was determined by:

$$V_r = \pi {R_r}^2 l_r \tag{3.16}$$

Where:

V_r is the volume of the reservoir (mm^3)

c. Total height of the reservoir from floor level

The reservoir and the chamber were elevated above the chiller in order to facilitate the pumping of the water from the reservoir to the chamber through the chiller and for effective return of the water to the reservoir by gravity; to enhance uninterrupted circulation. Hence, the total height of the reservoir was determined from equation 3.18.

$$H_r = l_r + h_r \quad (3.17)$$

Where:

H_r is total height of the reservoir (mm),

h_r is the height of the reservoir stand (mm)

3.4.4 Design of corrosion rig chamber

The corrosion rig chamber was designed by considering the size of the tensile sample that was used for investigation as the samples tested would be completely immersed in seawater. The dimension of the tensile sample designed according to the specifications in ASTM E8 was determined to be 150.8 mm long and 40 mm wide. The dimension of the tensile sample informed the design of the chamber. The size of the corrosion chamber was therefore scaled-up to accommodate a number of the tensile samples and for easy accessibility during experimental investigation.

a. Area of the chamber

The area of the corrosion chamber was determined by considering it as a six-faced rectangular box and according to the relationship given in Equation 3.6 (Ugwu, 2012). To determine the area of the corrosion chamber, Equation 3.6 was re-expressed as

$$A_{ch} = 2(XZ) + 2(XY) + 2(ZY) \quad (3.18)$$

Where:

A_{ch} is the area of the chamber (mm^2)

X is the length of the chamber (mm),

Y is the height of the chamber (mm)

Z is the width of the chamber (mm)

b. Volume of the chamber

Similarly, the volume of the corrosion chamber was determined as:

$$V_{ch} = XYZ \tag{3.19}$$

Where V_{ch} is the volume of the chamber (mm^3)

c. Total height of the chamber from floor level

As mentioned earlier, the chamber was elevated above the chiller in order to enhance effective return of the water to the reservoir by gravity. The total height of the chamber was therefore determined as:

$$H_{ch} = Y + h_{ch} \tag{3.20}$$

Where:

H_{ch} is total height of the chamber from floor level (mm),

h_{ch} is height of the chamber stand (mm).

3.5 Design Calculations

3.5.1 Determination of the properties of the refrigerating system

The values gotten from psychrometric tables and charts for refrigerant R-22 are:

Operating temperature = -15 ºC to 30 ºC (258K to 303K);

Critical temperature = 96 ºC (369K);

Critical pressure = 49.38 bar.

The operating condition was chosen for condenser temperature of 52 ^{o}C and evaporator temperature of 5 ^{o}C. Therefore, from the P-h chart of R-22, the following properties were obtained:

h_1 (Enthalpy of vapour refrigerant at the entrance of the compressor) = 405 kJ/kg

h_2 (Enthalpy of vapour refrigerant at discharge of the compressor) = 445 kJ/kg

$h_3 = h_4$ (Enthalpy of refrigerant at the discharge of the expansion valve) = 262 kJ/kg

Condenser pressure = 5.56 bar

Evaporator pressure = 22.12 bar

3.5.2 Determination of work done per kg of the refrigerant

The workdone per kg of the refrigerant was determined using Equation 3.1 as:

$$w = h_2 - h_1$$

w = 445-405 = 40 kJ/kg

3.5.3 Determination of the refrigerating effect

The refrigerating effect R_E, which is the heat absorbed by the refrigerant effect was obtained using Equation 3.2 as:

$$R_E = h_1 - h_4 = h_1 - h_{f3}$$

$h_4 = h_{f3}$, therefore,

R_E = 405 – 262 = 143 kJ/kg

3.5.4 Determination of coefficient of performance of the refrigerating system

Using Equations 3.3 or 3.4, the coefficient of performance of the refrigerating system was determined as

For a vapour compression cycle, the coefficient of performance (C.O.P) is determined by Equation 3.3 as:

$$C.O.P = \frac{Refrigerating\ effect}{Work\ done} = \frac{R_E}{w}$$

$$C.O.P = \frac{143}{40} = 3.58$$

(i) Design of chiller cabinet

a. Area of the chiller cabinet

Using Equations 3.5 and 3.6 the area of the chiller cabinet was determined as

Area = (two up and down faces) + (two front and back faces) + (two side faces)

$$A_c = 2(LW) + 2(LH) + 2(WH)$$

$$A_c = 2(598\ X\ 460) + 2(598\ X800) + (460\ X800)$$

A_c = 2242960 mm^2 = 2.243 m^2

b. Volume of the cabinet

Using Equation 3.7, the volume of the cabinet was determined as:

$$V_c = L\ x\ W\ x\ H$$

$$V_c = 598\ X\ 460\ X\ 800$$

V_c = 2.2006 X10^8 mm^3 = 0.22 m^3

c. Area of the chilling chamber

The total surface area of the chiller chamber was determined using Equation 3.8 as:

$$A_{CC} = 2\pi(R_o + r_i)(R_o - r_i + l_c)$$

$A_{CC} = 2\ X\ 3.142\ X\ (175 + 155)(175 - 155 + 460)$

A_{cc} = 995385.6 mm^2 = 0.954 m^2

d. Volume of the chilling chamber

Using Equation 3.10, the volume of the chilling chamber was determined as:

$V = \pi r^2 h$

$V = 3.143\ X\ 155^2\ X\ 460$

V = 3.47 *X* 10^7 mm^3 = 0.0347 m^3

e. Mass flow rate

The mass flow rate of the system was determined using Equation 3.13 (Ugwu 2012) as:

$M = \frac{V_c}{R_E}$

$M = \frac{0.0347}{143}$

M = 2.43 X 10^{-4} $kJ^{-1}kgm^3$

f. Capacity of the condenser

Using Equation 3.14, the capacity of the condenser was determined as (Ugwu 2012):

$C_c = M(h_2 - h_3)$

$C_c = 2.43\ \text{X}\ 10^{-4}\ \text{X}\ (445 - 262)$

C_c = 4.44 X 10^{-2} *TR* (Tonnes of refrigeration)

g. Capacity of the evaporator

Using Equation 3.15, the capacity of the evaporator was determined as (Ugwu, 2012):

$C_e = M(h_1 - h_4)$

$C_e = 2.43 \text{ X } 10^{-4} \text{ X}(405 - 262)$

C_e = 0.0347 kJ

(ii) Design of corrosion rig reservoir

a. Area of the reservoir

The area of the plastic reservoir was determined using the area of a cylinder expressed in Equation 3.16 as:

$A_r = 2\pi R_r l_r$

$A_r = 2\ X\ 3.142\ X\ 220\ X\ 510$

A_r = 705064.8 mm^2 = 0.71 m^2

b. Volume of the reservoir

The volume of the reservoir was determined using Equation 3.17 as:

$V_r = \pi {R_r}^2 l_r$

$V_r = 3.142\ X\ 220^2\ X\ 510$

Where:

V_r = 7.76 X 10^7 mm^3 = 0.0776 m^3

c. Total height of the reservoir from floor level

The total height of the reservoir was determined using Equation 3.18 as:

Total Height = Height of the reservoir + Height of the reservoir stand

Mathematically Equation 3.18 is expressed as:

$$H_r = l_r + h_r$$

$$H_r = 530 + 830$$

Where:

H_r = 1360 mm

(iii) Design of corrosion rig chamber

a. Area of the chamber

Using Equation 3.19, the area of the corrosion chamber was determined as (Ugwu, 2012):

$$A_{ch} = 2(XZ) + 2(XY) + 2(ZY)$$

$$A_{ch} = 2(245\ X\ 270) + 2(245\ X\ 260) + 2(270\ X\ 260)$$

Where:

A_{ch} = 400100 mm^2 =0.4 m^2

b. Volume of the chamber

The volume of the corrosion chamber was determined using Equation 3.20 as:

$$V_{ch} = X * Y * Z$$

$$V_{ch} = 245\ X\ 260\ X\ 270$$

Where V_{ch} 1.72 X 10^7 mm^3 =0.0172 m^3

c. Total height of the chamber from floor level

The total height of the chamber was determined using Equation 3.21 as:

$H_{ch} = Y + h_{ch}$

$H_{ch} = 260 + 1400$

H_{ch} = 1660 mm

3.6 Materials Selection

Locally sourced materials were used for the fabrication of the components of the corrosion rig in order to reduce costs. Since seawater was used for the corrosion experiments, consideration was given to the most important components such as the reservoir, specimens (corrosion) chamber, chilling chamber and pumps. These components are described as follows:

i. The reservoir was made of two concentric plastic buckets to create air gap insulation in order to avoid temperature losses and to avoid the reaction of the reservoir with the seawater
ii. The corrosion chamber was made of 5 mm thick Perspex box to ensure the visibility of the specimens when the corrosion process begins
iii. The chilling chamber of the corrosion rig was fabricated using stainless steel to avoid possible reaction with seawater during testing.
iv. Alphacool 12 volts pumps of the rate 4 litres per minute capacity were also plastics
v. The pipes conveying the seawater from the reservoir through the chiller to the corrosion chamber were also plastics.

Mild steel was used for the construction of the body frame of the corrosion chamber while the other components are ½ hP compressor with R-22 refrigerant, condenser, evaporator, expansion

CHAPTER FOUR

RESULTS AND DISCUSSION

4.1 Material Characterisation and Spectroscopic Analysis of the Steel

The chemical composition obtained from spectroscopic analysis that was conducted at Osogbo machine tools on X70 steel sample, as described in chapter three is set out in Table 4.1. The chemical composition that was conducted by the steel manufacturers as stated on the material certificate are shown in Table 4.2. It can be seen that the composition presented in both tables are similar considering all the elements. The marginal differences in compositions may be due to experimental errors. The implication of this is that it has been established that the material tested is in compliance with the API requirements. The comparison made with the material composition presented by Leonardo *et al.,* (2014) in Table 2.2 also shows similarity with the present material. The variation in some elements particularly in silicon may be due to difference in fabrication procedure by the steel manufacturers. The chemical composition of the filler material used for welding are presented in Table 4.3.

Table 4.1: Chemical composition of X70 steel (Osogbo)

Elements:	C	Si	Mn	P	S	Cr	Ni	Cu	Al
% Composition:	0.043	0.149	1.51	0.001	0.003	0.228	0.005	0.002	0.017
Elements:	V	Mo	Ti	Nb	N	Ca	Fe		
% Composition:	0.014	0.098	0.020	0.051	0.004	0.0022	97.8528		

Table 4.2: Chemical composition of X70 steel (Material certificate)

Elements:	C	Si	Mn	P	S	Cr	Ni	Cu	Al
% Composition:	0.05	0.210	1.560	0.006	0.002	0.250	0.010	0.010	0.049
Elements:	V	Mo	Ti	Nb	N	Ca	Fe		
% Composition:	0.030	0.160	0.020	0.070	0.004	0.0022	97.5664		

Table 4.3: Chemical composition of filler material

Elements	C	Si	Mn	P	S	Cr	Ni	Mo	Al	Cu	V
Weight (%)	0.12	0.16	0.85	<0.01	<0.01	0.04	0.03	0.46	<0.01	0.01	<0.01

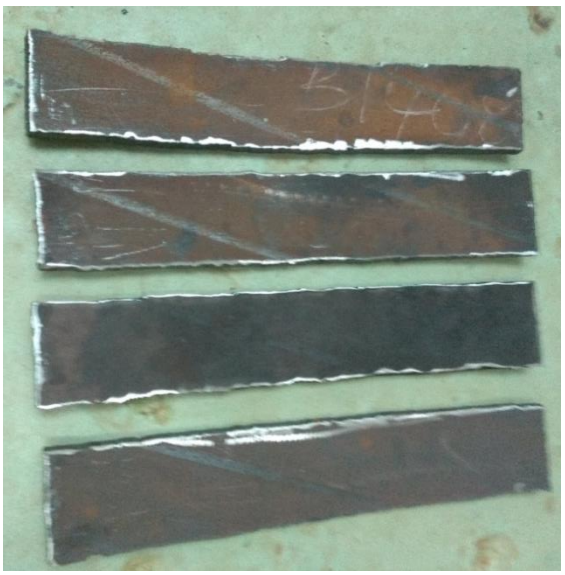

Plate X: API X70 steel plates

The API X70 steel plates before the welding was carried out are shown in Plate X, while Plate XI shows the welded plate.

Plate XI: Welded API X70 steel plate

4.2 Results of Microstructure Examination

The microstructure conducted at three different magnifications X100, X200 and X400 is presented in Plate xii while the micro images of the fracture surfaces of parent, weld and HAZ materials are shown in plate XII.

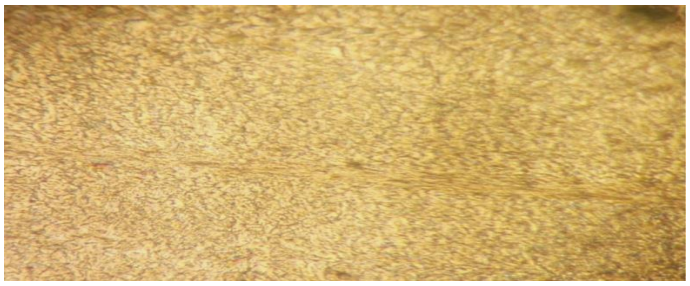

(a)

(b)

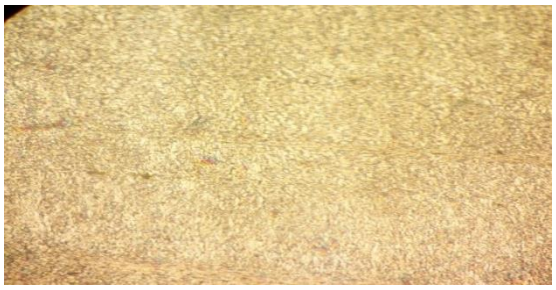

(c)

Plate XII: Microstructure of API X70 steel (a) Magnification: 400X (b) Magnification: 200X (c)Magnification: 100X

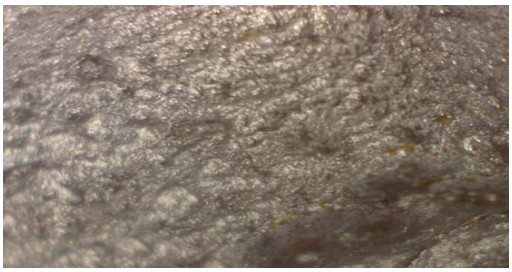

(a)

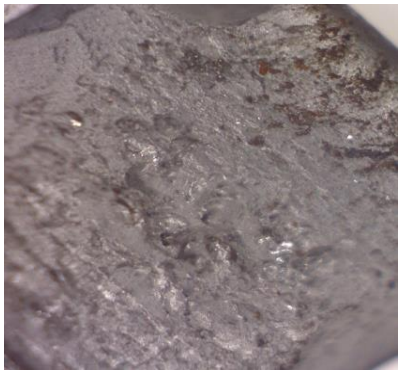

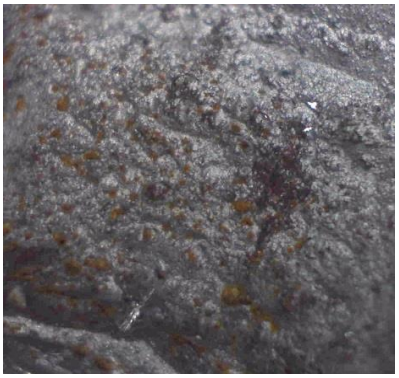

(b) (c)

Plate XIII: Micro images of fracture surfaces of (a) parent material, (b) weld, (c) HAZ

4.3 Tensile Test Results

The tensile test sample tested has an actual length of 320 mm and thickness of 20.8 mm. Prior to tensile testing, the corresponding weight of the samples were taken; the average weight of the samples without seawater corrosion were obtained to be 1075 g, while the average weight of those that were soaked in water was determined to be 949 g.

Tensile test results for samples tested in air are shown in Table 4.4. The mean of yield strengths for parent and weld materials were found to be 560 MPa and 578 MPa respectively while the corresponding tensile strengths were determined to be 634 MPa and 674MPa respectively. For parent materials, these values are close to those reported in (Leonardo *et al.,* 2014) where yield and tensile strengths for API X70 steel were reported to be 586 MPa and 640 MPa respectively.

In (Akonyi *et al.,* 2020), tensile test result for the similar weld material was obtained to be 660 MPa. It can be observed that this value is close to 674 MPa as obtained in this work. However, the difference may be due to dissimilar in weld procedure used in both cases. Further comparison was made with results reported in (Ike *et al*., 2019) show good agreement with those reported in this work for both parent and weld materials. The HAZ dimension was averagely 2.5 mm in width and due to the non-availability of machine that could test smaller tensile test specimens of such dimensions, tensile tests for HAZ were not carried out.

Table 4.4: Yield and Tensile strengths of samples tested in air

Number of tests	Yield Strength (MPa)		Tensile strength (MPa)		Elongation (%)	
	Parent material	Weld materials	Parent material	Weld materials	Parent material	Weld materials
1	568.55	582.12	645.86	672.14	35	34
2	576.86	587.76	624.75	655.15	35	35
3	556.36	576.15	636.14	698.13	36	33
4	547.96	575.23	624.18	657.19	32	34
5	553.25	571.76	647.35	685.23	33	35

In Table 4.5, tensile test results for samples immersed in seawater are presented. The mean of yield strength results for parent and weld materials were obtained to be 428 MPa and 416 MPa and the corresponding tensile strengths were determined to be 512

MPa and 529 MPa respectively. It can be observed that yield strength of parent materials soaked in seawater are higher than those in weld materials as against what was obtained for samples tested in air. Due to material variability in weld, this may be due to detrimental effect of corrosion in weld materials compared to in parent materials. In Ike et al. work (Ike *et al.,* 2019), the yield strength for weld samples was obtained to be 609 MPa as against 416 MPa in this work. The difference in these results could be due to the effect of soaking time. In this study, tensile samples were soaked for 12 months before testing while in (Ike, *et al.,* 2018) work, samples were soaked for 12 weeks. Therefore, due to time dependent mechanics associated with seawater corrosion, such difference should be expected.

Table 4.5: Yield and Tensile strengths of samples soaked in seawater

Number of tests	Yield Strength (MPa)		Tensile strength (MPa)		Elongation (%)	
	Parent material	Weld materials	Parent material	Weld materials	Parent material	Weld materials
1	432.58	412.01	489.57	529.66	22.1	21.8
2	428.47	417.89	494.35	532.60	23.1	21.4
3	432.18	414.95	526.72	529.66	22.7	22.5
4	426.89	423.01	544.37	523.76	23.6	21.6
5	421.49	413.03	505.24	530.65	24.6	21.8

4.4 Impact Test Results

Due to the dimension of HAZ, it was possible to align HAZ in the notch of charpy test specimens. The results of HAZ charpy energies in air are compared with those obtained in parent and weld materials in Table 4.6. It can be seen that charpy energy values are higher in parent than in HAZ and with weld materials having the lowest values. Variability in material microstructure in weld material may be responsible for the lower charpy values. For the five samples tested in air, there is no significant difference in the values. The lower energy in weld may also be attributed to tensile residual stresses in the weld during manufacturing; therefore it is possible that the tip of the notch was close to the damaging part of the residual stresses in the materials. However, residual stresses may also be present in the HAZ but this may be lower compared to those usually present in weld materials.

Table 4.6: Charpy impact energy for parent, weld and HAZ materials in air

		Impact Energy (J)	
Number of tests	Parent materials	Weld materials	HAZ
1	328.20	105.70	263.50
2	350.20	97.90	270.30
3	328.50	87.80	270.30
4	329.10	98.50	272.50
5	330.75	89.30	267.50

Charpy impact test results obtained in parent, weld and HAZ materials are presented in Table 4.7. The detrimental effect of seawater has shown to have influenced the impact tests results as can be observed in the table. The HAZ average charpy energy values obtained in seawater are approximately twice of those obtained in parent and weld materials respectively. Effect of seawater has significantly reduced the energies absorbed in the materials as compared to those tested in air (Table 4.6).

Table 4.7: Charpy impact energy for parent, weld and HAZ materials in seawater

	Impact Energy (J)		
Number of tests	Parent materials	Weld materials	HAZ
1	158.50	72.40	123.40
2	160.30	56.60	145.50
3	175.20	50.90	165.40
4	177.60	58.20	155.70
5	180.50	46.50	132.20

4.5 Compression Test Results

Compression test was carried out at the Obafemi Awolowo University (OAU) Ile Ife using Instron Testing Machine. Results obtained for parent and weld materials are shown in Table 4.8 where it can be seen that the maximum compressive stresses for parent and weld materials are similar. However, compressive strain and energy absorbed at maximum compressive stresses revealed higher values in parent materials

than in weld. The mean compressive stresses for the parent and weld steel plates were obtained to be 750.08 MPa and 750.38 MPa. Recently, compressive stress results for parent and weld API X70 steel plates were obtained to be 1393.7 MPa and 1902.1 MPa (Erinfolami and Adedipe, 2021). However, these values were obtained numerically using ANSYS, where those reported in this research were obtained experimentally; therefore, this may be the reason for the difference in results. Another reason may be due to volumetric effect arising from the sizes of samples used for testing. According to Erinfolami and Adedipe, (2021), the length of the sample used was 60 mm with a width of 20 mm while in this study, 20 mm by 20 mm was used. Therefore, volumetric effect in the higher sample could result in higher compressive stress.

Table 4.8: Results of compressive test in air

Maximum compressive stress (MPa)		Maximum compressive strain (%)		Energy at maximum compressive stress (J)	
Parent	Weld	Parent	Weld	Parent	Weld
750.01	750.05	26.95	16.57	63.19	42.66
750.03	750.09	26.87	16.86	63.21	42.78
750.05	751.00	26.98	16.88	63.23	42.57

Table 4.9 shows the compressive test results for parent and weld materials in seawater with the corresponding maximum strain and energies at maximum compressive stresses. It can be observed that there are significant reductions in the values compared to those obtained in air (Table 4.8) due to the effect of seawater corrosion.

Table 4.9: Results of compressive test in seawater

Maximum compressive stress (MPa)		Maximum compressive strain (%)		Energy at maximum compressive stress (J)	
Parent	Weld	Parent	Weld	Parent	Weld
455.15	423.30	11.25	9.50	38.25	21.75
456.30	421.15	11.65	9.01	38.05	22.00
455.33	424.03	11.75	9..00	38.75	21.18

4.6 Hardness Test Results

Hardness values were taken from 33 points on the specimen as shown in Figure 4.1. Points 1 to 11 are the top of the weld specimen; points 12 to 22 are the middle while points 23 to 33 are the bottom of the plate.

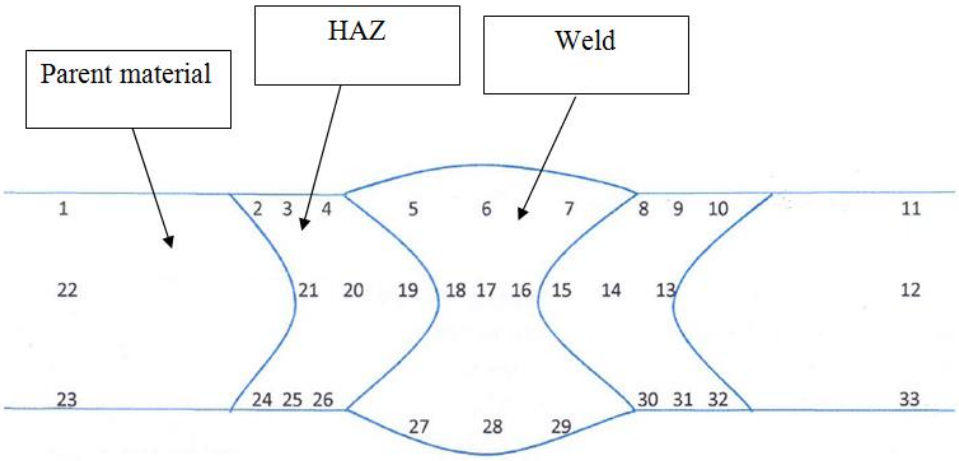

Figure 4.1: Schematic diagram of hardness test sample

Hardness values were taken on parent, weld and HAZ as indicated in the figure. The hardness values of the 33 points are plotted in Figure 4.2.

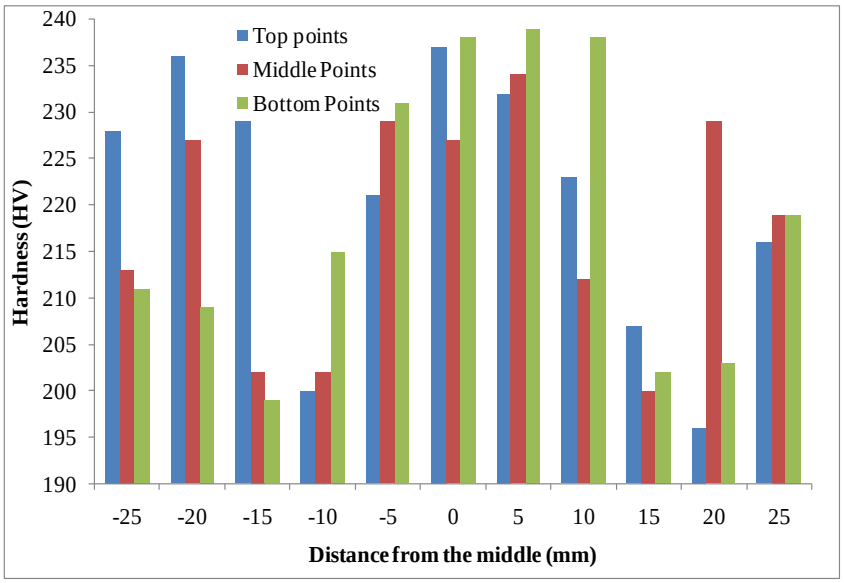

Figure 4.2: Vickers hardness values

The top of the plate revealed the hardness value with a mean hardness value of 221 HV, while the middle and bottom of the plate have mean hardness value of 218 HV and 219 HV respectively. The hardness value of the HAZ decreases from the region closer to the weld (points 4, 19 and 26) towards the parent material (points 2, 21 and 24). This was also applicable to the hardness of the right side of Figure 4.1. The highest hardness of 239 HV value was obtained in weld at point 29, while the minimum hardness of 196 HV was obtained in parent material at point 11. These results are in agreement with hardness value measured in similar material (API X 70 steel) as hardness values were higher in weld than in parent material (Ike *et al.*, 2019).

4.7 Results of SEM Analysis

Analysis of fracture surfaces of the specimens were carried out at OAU Ile Ife. Specific areas of the fractured specimens were analysed to reveal the type of failure mechanisms for those tested in air and seawater. Figure 4.3 shows the fractures surfaces of charpy parent materials tested in air and seawater. In air (Figure 4.3 a) the fracture surfaces shows a mixture of ductile and brittle failure mechanism. However, in seawater, some corrosion products are deposited on the surfaces after testing. Some dimples can also be observed as shown in Figure 4.3 b.

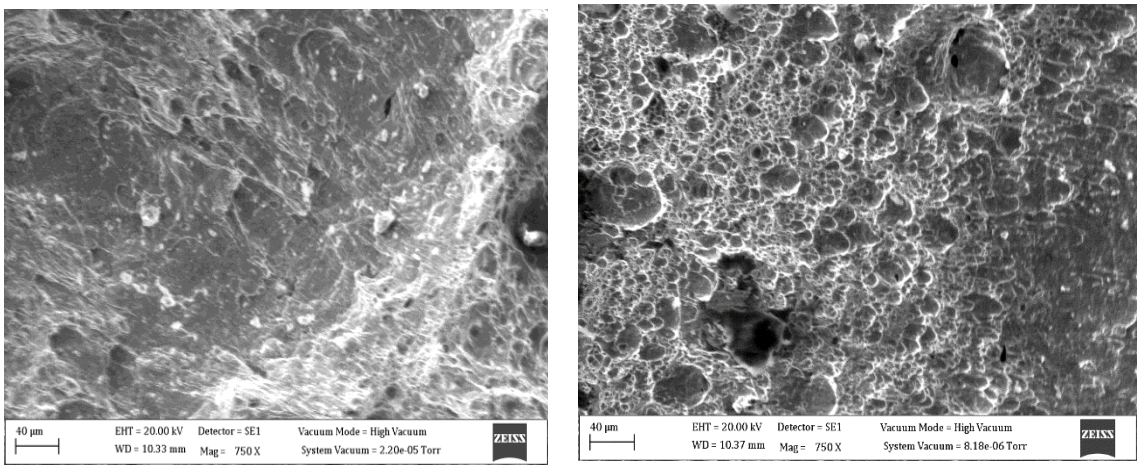

(a) **(b)**

Figure 4.3: Fracture surface of charpy parent materials: (a) air (b) seawater

Fracture surfaces of weld samples tested in air and seawater are shown in Figure 4.4 where cleavage mechanism can be seen in the sample tested in air (Figure 4.4 a). The cleavage could be due to defects within the weldment material variation in the weld. In the sample tested in seawater (Figure 4.4 b) revealed corrosion products on the surface with ductile fracture mechanisms.

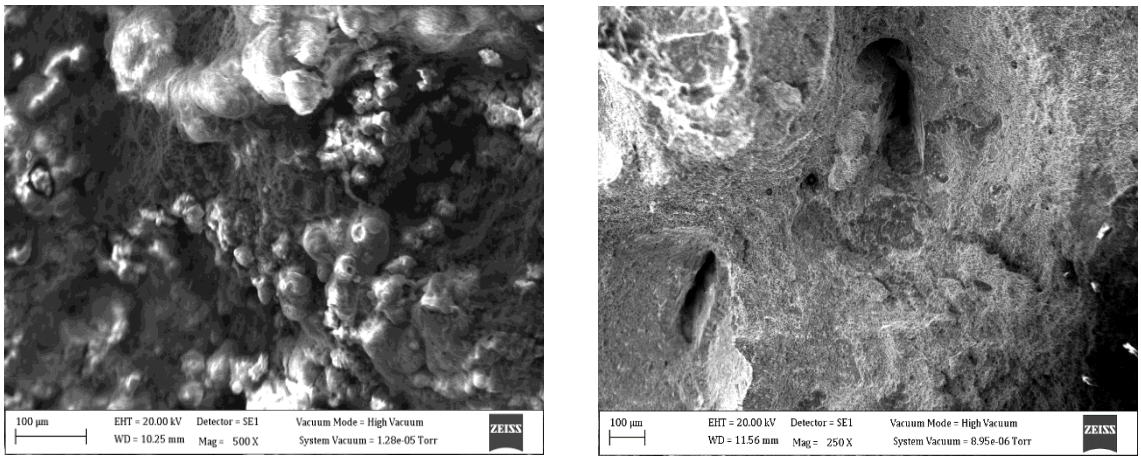

(a) **(b)**

Figure 4.4: Fracture surface of charpy weld materials: (a) air (b) seawater

The fracture surfaces of charpy HAZ materials tested in air and in seawater are shown in Figure 4.5 a and b. Brittle fracture mechanisms was observed as the nature of the fracture surface while the sample tested in seawater exhibited corrosion pits due to the effect of seawater. The severity of the corrosion pit was more near notch of the charpy specimen due to direct exposure of the notch during soaking.

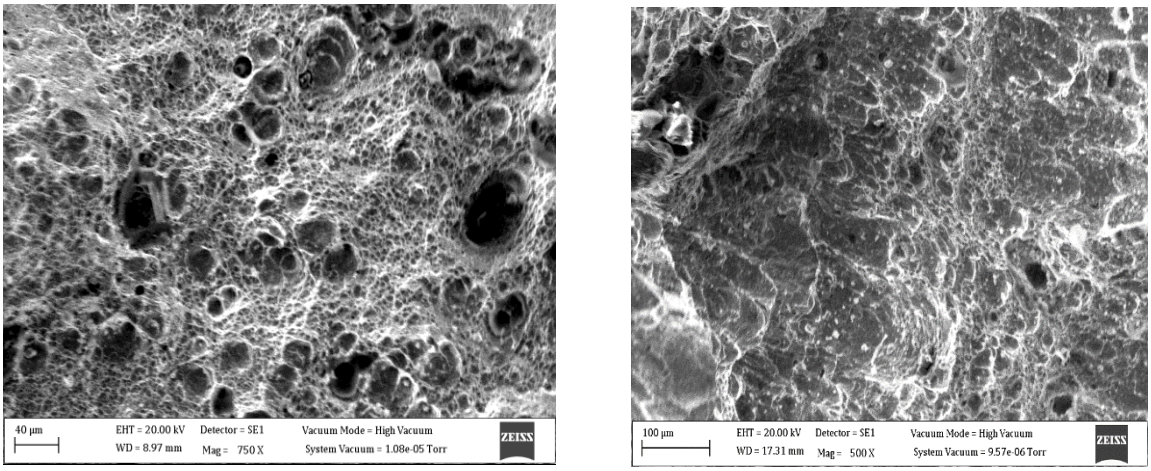

(a) **(b)**

Figure 4.5: Fracture surface of charpy HAZ materials: (a) air (b) seawater

Figure 4.6 shows the fracture surfaces of tensile samples tested in air and in seawater. The air sample (Figure 4.6a) revealed majorly ductile fracture which is peculiar to tensile failure under monotonic loading.

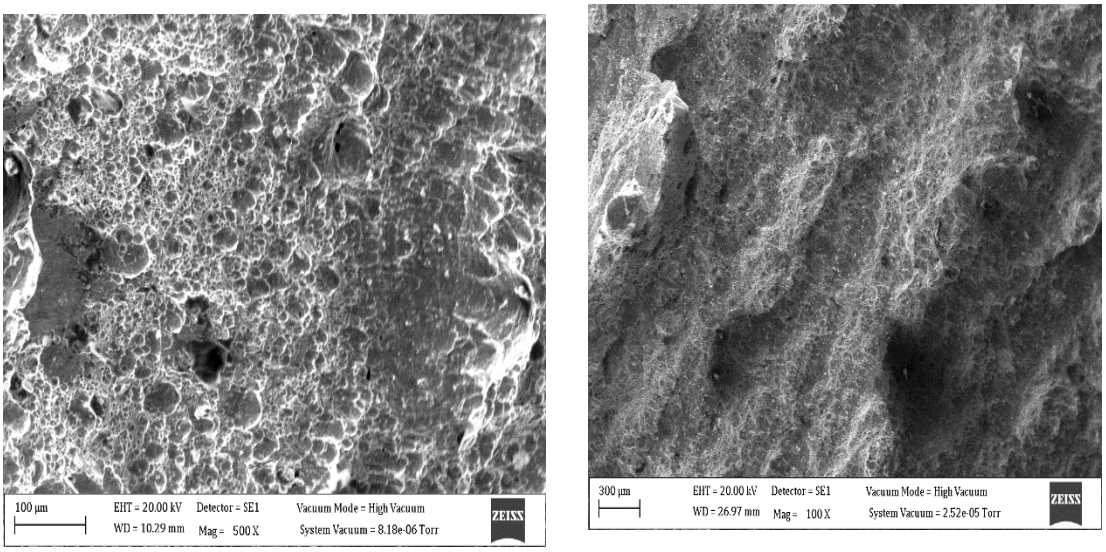

(a) **(b)**

Figure 4.6: Fracture surface of tensile parent materials: (a) air (b) seawater

The seawater sample (Figure 4.6b) shows a mixture of brittle and ductile fracture. Some pits are also evident in the Figure.

The fracture surfaces of tensile weld samples are shown in Figure 4.7. The fracture surface of the air sample revealed ductile fracture with some tearing as can be observed in Figure 4.7a. The appearance of the fracture surface could be attributed to the effect of material microstructure and possible welding defect. The fracture surface of seawater sample (Figure 4.7 b) was covered by corrosion products arising from the effect of seawater as shown in the Figure.

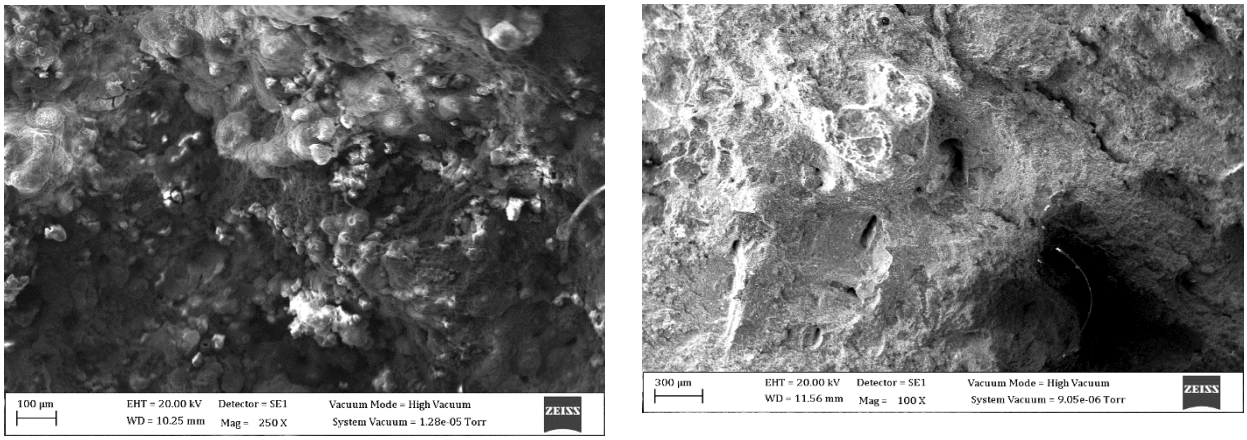

(a) **(b)**

Figure 4.7: Fracture surface of tensile weld materials: (a) air (b) seawater

4.8 Result of X-rayDiffraction (XRD)

The XRD analysis was carried out using Miniflex XRD Rigadu machine at OAU Ile Ife. The XRD patterns obtained from the materials are shown in Figure 4.8 on a 2Ɵ scale.

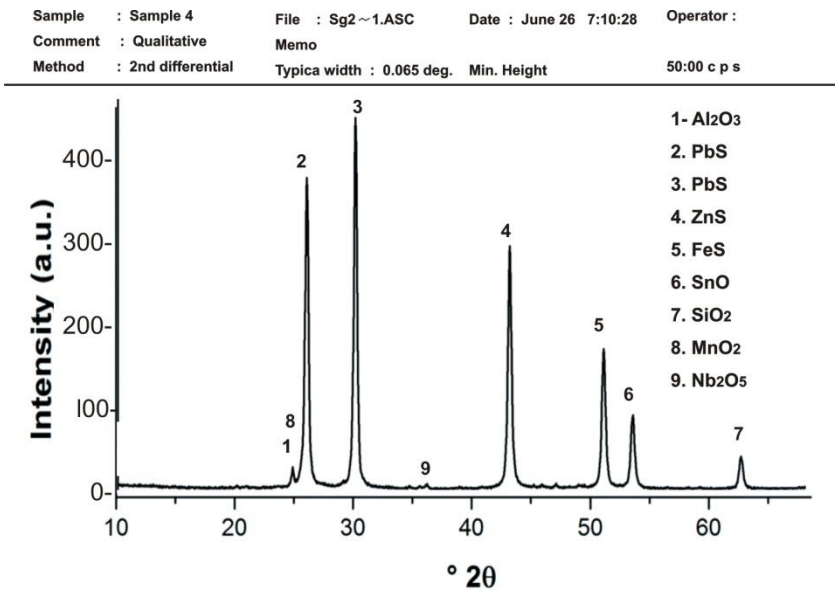

Figure 4.8: Result of XRD analysis

The maximum peaks (2 and 3) is characterized by the presence of lead sulphide with the lowers peak (peak 1) shows the presence of aluminium oxide in the material.

4.9 Environmental Reduction Factor (ERF)

Environmental reduction factors have been determined to compare the extent to which the effect of seawater has influenced the tensile, impact and compressive properties of the material tested. The ERFs were determined by dividing the selected properties of the material in air with the seawater ones. The ERFs for tensile parent materials are given in Table 4.10 where it can be seen that the EFRs are in the range of 1.1 to 1.3 with an approximately mean value obtained to be 1.2. This implies that in this case, the effect of seawater corrosion has reduced the tensile properties of parent materials by a factor of 1.2.

Table 4.10: ERF in tensile specimens

Tensile strength (MPa)		ERF	Tensile Strength (MPa)		ERF
PM (air)	PM (SW)		WM (air)	WM(SW)	
645.86	489.57	1.3	672.14	529.66	1.3
624.75	494.35	1.3	655.15	532.60	1.2
636.14	526.72	1.2	698.13	529.66	1.3
624.18	544.37	1.1	657.19	523.76	1.3
647.35	505.24	1.3	685.23	530.65	1.3

PM: Parents materials, WM: Weld materials, SW: Seawater

Similarly, in weld materials (Table 4.10), the ERFs are in the range of 1.2 and 1.3 with an approximately mean value obtained to be 1.3 which shows that seawater influenced

the tensile properties of the weld materials by a factor of 1.3. However, value of ERFs may entirely depend of several factors which include soaking time and test temperature, but the results presented were obtained using a soaking time of 12 months. In (Ike *et al.*, 2018), weld tensile materials were soaked for 12 weeks and the percentage reduction in tensile strength in air compared to in seawater at was determined to be 10.5 %. This value is relatively minimal compared to the determined ERF of 1.3 and this has shown the effect of soaking time.

Table 4.11 shows the determined ERFs for charpy specimens tested using impact tests. The ERFs were determined for parent, weld and HAZ materials.

Table 4.11: ERF in charpy specimens

Impact Energy (J)		ERF	Impact Energy (J)		ERF	Impact Energy (J)		ERF
PM (air)	PM (SW)		WM (air)	WM(SW)		HAZ (air)	HAZ (SW)	
328.20	158.50	2.1	105.70	72.40	1.5	263.50	123.40	2.1
350.20	160.30	2.2	97.90	56.60	1.7	270.30	145.50	1.9
328.50	175.20	1.9	87.80	50.90	1.7	270.30	165.40	1.6
329.10	177.60	1.9	98.50	58.20	1.7	272.50	155.70	1.8
330.75	180.50	1.8	89.30	46.50	1.9	267.50	132.20	2.0

PM: Parents materials, WM: Weld materials, HAZ: Heat affected zone, SW: Seawater

The ERFs for parent materials are in the range of 1.8 and 2.2 which the mean value of approximately 2.0; and those for weld materials are in the range of 1.5 to 1.9 which the mean value of approximately 1.7. Similarly, the ERFs for HAZ materials are in the range of 1.6 to 2.1 which the mean value of approximately 1.9. These results are higher

than the determined ERFs for tensile materials. The higher ERFs in charpy specimens may be due to the size of the specimen and the artificial defects in form of the notch in the specimens. It is expected that charpy specimens because of the notch, would be more exposed to seawater than tensile specimens and this may result in higher ERFs. However, similar results have not been found in the literature comparing the ERFs in parent, weld and HAZ.

The ERFs of parent and weld compression specimens are compared in Table 4.12 and it can be observed that the ERFs are higher in weld than in parent materials for the tests carried out. The results are in the range averagely in the range of 1.6 and 1.7 for parent materials and ERFs for weld materials were obtained to be 1.8.

Table 4.12: ERF in compression specimens

Maximum compressive stress (MPa)			Maximum compressive stress (MPa)		
PM (air)	PM (SW)	ERF	WM (air)	WM(SW)	ERF
750.01	455.15	1.7	750.05	423.30	1.8
750.03	456.30	1.6	750.09	421.15	1.8
750.05	455.33	1.7	751.00	424.03	1.8

PM: Parents materials, WM: Weld materials, SW: Seawater

The mean ERFs are approximately 2.0 in both cases which imply that the effect of seawater corrosion on compressive properties of API X70 steel in this case is a factor of 2. In (Ike *et al.*, 2019), percentage reduction in compressive properties of API X70 steel due to the effect of seawater was obtained to be 18.7 %,where in this study, ERF of 2.0

may be related to a percentage reduction of approximately 50 %. The higher value could be due to the effect of soaking time as mentioned previously.

4.10: Results of Corrosion Rig Assemble and Coefficient of Performance

The results obtained from the design analysis and calculations show that the developed corrosion rig chiller has a coefficient of performance (COP) of 3.58. This value conforms with the recommendation for COP in (Khurmi and Gupta 2016). The determined COP has shown that the chiller's COP is consistent to those of vapour compression refrigeration systems of similar refrigerant. Using the Equations in section 3.4, the determined corrosion rig parameters and the corresponding results are summarized in Table 4.13.

Table 4.13: Calculations of corrosion rig parameters and results

Determined Parameters	Results
Work done per kg of refrigerant (w)	Using Equation 1, w = 445-405 = 40 kJ/kg
Refrigerating effect (R_E)	Using Equation 2, R_E = 405 – 262 = 143 kJ/kg
Coefficient of performance of the refrigerating system ($C.O.P$)	Using Equation 3, $C.O.P = \frac{143}{40}$= 3.58
Area of the chiller cabinet (A_c)	Using Equation 6 $A_c = 2(598\ X\ 460) + 2(598\ X800) + (460\ X800)$ A_c = 2242960 mm^2 = 2.243 m^2
Volume of the cabinet (V_c)	Using Equation 7 V_c = 2.2006 X10^8 mm^3 = 0.22 m^3
Area of the chilling chamber (A_{cc})	Using Equation 9 $A_{CC} = 2\ X\ 3.142\ X\ (175 + 155)(175 - 155 + 460)$ A_{cc} = 995385.6 mm^2 = 0.954 m^2
Volume of the chilling chamber (V)	Using Equation 10

	$V = 3.143\ X\ 155^2\ X\ 460$
	V = 3.47 *X* 10^7 mm^3 = 0.0347 m^3
Mass flow rate(*M*)	Using Equation 13
	$M = \frac{0.0347}{143}$, M = 2.43 X 10^{-4} $kJ^{-1}kgm^3$
Capacity of the condenser (C_c)	Using Equation 14
	$C_c = 2.43\ X\ 10^{-4}\ X\ (445 - 262)$
	C_c = 4.44 X 10^{-2} *TR* (Tonnes of refrigeration)
Capacity of the evaporator (C_e)	Using Equation 15
	$C_e = 2.43\ X\ 10^{-4}\ X(405 - 262)$
	C_e = 0.0347 kJ
Area of the reservoir (A_r)	Using Equation 16
	$A_r = 2\ X\ 3.142\ X\ 220\ X\ 510$
	A_r = 705064.8 mm^2 = 0.71 m^2
Volume of the reservoir (V_r)	Using Equation 17, $V_r = 3.142\ X\ 220^2\ X\ 510$
	V_r = 7.76 X 10^7 mm^3 = 0.0776 m^3
Total height of the reservoir from floor	Using Equation 18, $H_r = 530 + 830$
level (H_r)	H_r = 1360 mm
Area of the chamber (A_{ch})	Using Equation 19
	$A_{ch} = 2(245\ X\ 270) + 2(245\ X\ 260) + 2(270\ X\ 260)$
	A_{ch} = 400100 mm^2 =0.4 m^2
Volume of the chamber (V_{ch})	Using Equation 20
	$V_{ch} = 245\ X\ 260\ X\ 270$
	V_{ch} = 1.72 X 10^7 mm^3 = 0.0172 m^3
Total height of the chamber from floor	Using Equation 21
level (H_{ch})	$H_{ch} = 260 + 1400$, H_{ch} = 1660 mm

Figure 4.9 shows the front view of the developed rig with the obtained dimensions in mm. These dimensions were obtained from the analyses that are reported in section 3.4.

The mode of operation of the corrosion rig explained as follows: First, the seawater was pumped from the reservoir to the chiller through a pump. In the chilling chamber, the temperature of the seawater was reduced to the target temperature used for testing. This was assisted by electrical control unit equipped with temperature display of the chiller. Then the water was pumped from the chiller to the chilling chamber where corrosion takes place. At the level of the return pipe attached to the corrosion chamber, the water returns to the reservoir by gravity and the process continues as a loop.

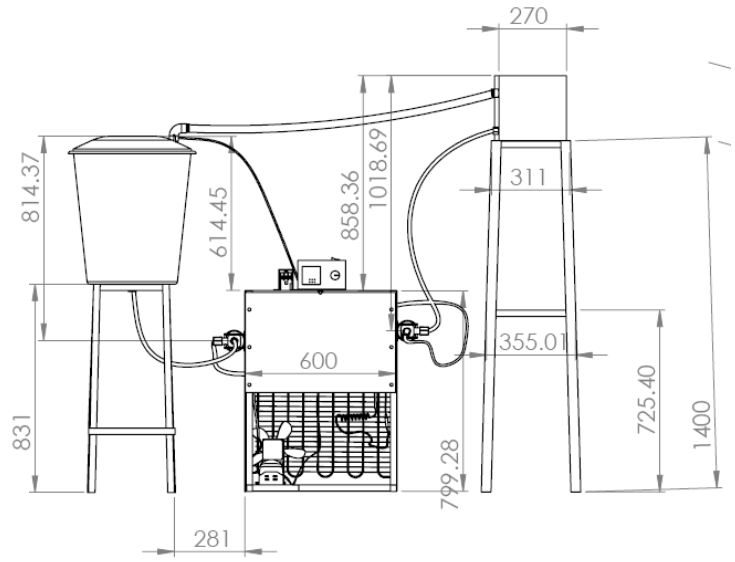

Figure 4.9: Front view of the developed corrosion rig

(a) (b)

Plate XIV: (a) Developed corrosion rig (b) Corrosion rig chamber

(a) (b)

Plate XV: (a) chiller (b) Corrosion chamber with samples immersed in seawater

In Plate XIV (a), the corrosion rig assembly is shown while Plate xiv (b) shows the corrosion chamber with samples immersed in seawater. Plate xv (a) shows the chiller. The brownish colour of the water can be seen in Plate xv (b) which implies effect of corrosion. The samples were visible within the first week of testing while from the second week, the seawater turned completely brown and hence the samples became invisible which implies that the interaction of the seawater with the API X70 steel was time dependent. Figure 4.12 shows the tensile samples immersed in seawater for 12 months before the tensile tests were carried out.

Plate XVI: Corroded Tensile Samples

CHAPTER FIVE

CONCLUSION AND RECOMMENDATIONS

5.1 Conclusion

The properties of parent, weld and heat affected zone of the steel pipeline were investigated. The following conclusions can be drawn from this research.

Characterization of the weldment revealed that the weld area and the HAZ depend on material thickness, heat input used during welding and possible effect of residual stresses in the weldment. The average dimension of the HAZ was obtained to be 2.5 mm. Chemical composition of the material compared well with those obtained from similar researches.

A laboratory scale corrosion rig for testing pipeline steel materials in seawater was developed using locally sourced materials. The coefficient of performance of the chiller was determined to be 3.58. This study has shown that locally sourced materials could be utilized to develop laboratory scale corrosion rig to simulate a similar seawater environment that pipelines could be subjected. The detrimental effect of seawater on the samples showed that the rig could be used for testing other steel materials.

The effect of seawater reduced the mechanical properties of the API X 70 steel pipeline with respect to the immersion time.. In air, the mean yield strengths for parent and weld materials were found to be 560 MPa and 578 MPa respectively while the corresponding tensile strengths were determined to be 634 MPa and 674MPa respectively. In seawater, the mean yield strength for parent and weld materials were obtained to be 428 MPa and 416 MPa and the corresponding tensile strengths were determined to be 512 MPa and 529 MPa respectively. Charpy energy values were

higher in parent than in HAZ and with weld materials having the lowest energy. The absorbed energies in the specimens were relatively lower in seawater than those tested in air. The effect of seawater was also applicable to the reduction in compressive stresses of the material. The hardness value of the HAZ decreases from the region closer to the weld towards the parent material. The highest hardness of 239 HV value was obtained in weld, while the minimum hardness of 196 HV was obtained in parent material. Fracture surfaces of the specimens showed the combination of brittle and ductile failure mechanisms.

The effect of seawater corrosion reduced the tensile properties of parent and weld materials by factors of 1.2 and 1.3 respectively. Environmental reduction factor of approximately 2.0 was obtained in charpy parent, weld and HAZ materials due to the effect of seawater. Seawater also reduced the compressive properties of parent and weld materials by factors of 1.7 and 1.8 respectively. This study has shown that environmental reduction factor depends on the immersion or soaking time.

5.2 Recommendations

The following are the recommendations made by the research:

i. The machine developed is recommended for a laboratory scale corrosion rig for testing pipeline steel materials in seawater using locally sourced materials.
ii. Indigenous research work like this should be motivated.
iii. The developed machine could be further calibrated with varying quantities of batching tests.
iv. Further research should investigate the Microstructure of the parent, weld and HAZ before and after tests. Tensile and compression tests should also be carried out on HAZ materials for compression with results of the present study.

v. Performances of other environmentally friendly refrigerants should be investigated on the developed corrosion rig as part of further research. Further studies should also investigate the corrosion fatigue behaviour of the APIX70 steel pipeline considering the seawater environment used in this research.

5.3 Contributions to Knowledge

The study provided a novel approach of establishing mechanical properties of API 5L X70 steel plates at parent, weldment and heat affected zones in air and seawater for optimum pridiction of corrosion failure of pipelines and their prevention strategy. Design parameters were also established for the development of a new laboratory-scale corrosion rig for the API 5L X70 steel plates.

REFERENCES

Adedipe, O. (2015). "*Integrity of Offshore Structures."* PhD Thesis, Cranfield University.

Adedipe, O., Feargal, B., & Athanasios, K. (2015). Corrosion Fatigue Load Frequency Sensitivity Analysis. *Marine Structures,* 42, 115–36

Akonyi, N. S., Olugboji O. A., Egbe, E. A. P., Adedipe, O. & Lawal, A. S .(2020). Optimization of Process Parameters for MAG Welding of API X70 Material to Predict Tensile Strength Using Taguchi Method. *Nigerian Journal of Technology,* 39 (4), 1100–1107

Aliu, S. (2012). Investigation of Mechanical and Microstructural Properties of Welded Joint of Nigerian National Petroleum Corporation Pipelines. M. Eng. Thesis, Federal University of Technology, Minna, Nigeria

Arya, J. S. & Chavda, N. K. (2014). Design and Performance Analysis of Water Chiller – A Research. *International Journal of Engineering Research and Applications,* 4 (6), 19–25

ASTM D1141, (2008). Standard Practice for the Preparation of Substitute Ocean Water.

ASTM E 23, (2014). Standard Test Methods for Notched Bar Impact Testing of Metallic Materials

ASTM E8 (2013). Standard Test Methods for Tension Testing of Metallic Materials

Austin, A. &Julian, A. (1994). The Role of Corrosion Fatigue Crack Growth Mechanisms in Predicting the Fatigue Life of Offshore Tubular Joints. PhD Thesis, University College London. PP, 12.

Ayou, D. S. & Coronas, A. (2020). New Developments and Progress in Absorption Chillers for Solar Cooling Applications. *Applied Sciences,* 10 (4073), 1–40. doi:10.3390/app10124073

Ayres, S. (2013). *Design of a 12 kW Air-Cooled Water Chiller*. MSc Thesis, University of Pretoria

Bagarella, G., Lazzarin, R . M. & Lamanna, B. (2013). Cycling Losses in Refrigeration Equipment. An Experimental Evaluation: *International Journal of Refrigeration,* 36 (8), 2111–2118

Bai, L., Gao, L. & Jiang, K. (2018). Corrosion Crack Nucleation Mechanism in the Welded Structures of X65 Steel in Natural Seawater. *Advances in Material Science and Engineering*, 1–14

Beech, I. & Sunner, J. (2004). Biocorrosion: Towards Understanding the Interaction between Biofilms and Metals. *Current Opinion in Biotechnology,* 15 (3), 181–86

Bolaji, A., Bukola, O., Ezra, A. A., Michael, R. A., Olanipekun, M. U., &

Emmanuel, A. (2019). Theoretical Investigation of Energy-Saving Potential of Eco-Friendly R430A, R440A and R450A Refrigerants in a Domestic Refrigerator. *Iranian Journal of Science and Technology, Transactions of Mechanical Engineering,* 43 (1), 103–12. doi:10.1007/s40997-017-0110-4.

Brondel, D., Edwards, R., Hayman, A., Hill, D., Mehta, S. & Semerad, T. (1999). Corrosion in the oil industry. *Oil Review, . 4*

Chen, X., Yuan, J., Huang, J., Ren, K., Liu, Y., Lu, S. & Li, H. (2014). Large-Scale Fabrication of Superhydrophobic Polyurethane/nano-Al_2O_3 Coatings by Suspension Flame Spraying for Anti-Corrosion Applications. *Applied Surface Science,* 311: 864–69. doi:https://doi. org/10.1016/j.apsusc.2014.05.186

Chen, Y., Zhang, H., Zhang, J., Li, X. & Zhou, J. (2015). Failure Analysis of High Strength Pipeline with Single and Multiple Corrosions. *Material Design,* 67 (552-557)

Cheng, Y. F. & Xue, H. B. (2011). Characterization of Inclusion of X80 Pipeline Steel and Its Correlation with Hydrogen-Induced Cracking. *Corrosion Science,* 53 (4), 1201–1208.

Choi, J. M. & Kim, Y. C. (2020). The Effects of Improper Refrigerant Charge on the Performance of a Heat Pump with an Electronic Expansion Valve and Capillary Tube. *Energy*, 27 (4), 391–404.

Cicek, V. & Al-numan, B. (2011). *Corrosion Chemistry*. 1st Editio. Hoboken, New Jersey.

Dexter, S. C. (2003). Microbiologically Influenced Corrosion. Metals Handbook: *Corrosion Fundamentals, Testing, and Protection*, Metals Park: ASM International.

Du Plessis, G. E., Arndt, D. C. & Mathews, E. H. (2015). The Development and Integrated Simulation of a Variable Water Flow Energy Saving Strategy for Deep-Mine Cooling Systems. *Sustainable Energy Technology,* 10, 71–78

ASTM., E384, (2012). Standard Test Method for Knoop and Vickers Hardness of Materials.

Eliyan, U., Faysal, F., El-sadig, M.& Akram, A. (2013). Investigating the Corrosion of API-X100 Pipeline Steel in Aerated Carbonate Solutions by Electrochemical Methods *International Journal of Electrochemical Science,* 8, 578–590

Fan, J .W., Luo, J., Gao, J. J., Bo, F. H., Ren, Q., Lin, X. H. & Geng, H. B. (2020). Mechanical Properties and Microstructure of Longitudinal Submerged Arc Welded Joint of a New C – Mn Steel Sheet Cladding Fine Grained Ferrite in Surface Layer for a Long Distance Transport Pipeline. *IOP Conference Series:Material Research Express,* 7 (046513), 1–13

Fong, K. F., Lee, C. K. & Chow, T. T. (2011). Improvement of Solar-Electric Compression Refrigeration System through Ejector-Assisted Vapour Compression Chiller for Space Conditioning in Subtropical Climate. *Energy and Buildings,* 43

(12), 3383–3390 doi:10.1016/j.enbuild.2011.08.038.

Fuadi, Z., Ardiyansyah, Y., Rachmah, R., Nyayu, A., Idrus, A., Budihardjo, B.& Nandy, P. (2019). Chiller Performance Study with Refrigerant R290. In *AIp Conference Proceedings, The 10th International Meting of Advances in Thermofluids*, 1–8. doi:https://doi.org/10.1063/1.5086608

Garbatov, Y,.C., Guedes, S., Parunov, J. & Kodvanj, J. (2014). Tensile Strength Assessment of Corroded Small Scale Specimens. *Corrosion Science*, 85, 296–303

Hadya, B. (2016). Analysis of Vapour Compression Refrigeration System with Sub-Cooling and Super Heating with Three Different Refrigerants for Air-Conditioning Applications. *International Journal of Engineering Science and Research Technology*, 5 (11), 70–77

Hillenbrand, H. G., Niederhoff, K., Amoris, E., Perdix, C., Streisselberger, A. & Zeislmair, U. (1999). Development of Linepipe in Grades Up to X100. *Europipe Technical Literature*. Washington.

Ijaola, O. A., Farayibi, P. K.& Asmatulu, E. (2020). Superhydrophobic Coatings for Steel Pipeline Protection in Oil and Gas Industries : A Comprehensive Review. *Journal of Natural Gas Science and Engineering*, 83. doi:10.1016/j.jngse.2020.103544.

Ike, T. M. (2018). Investigation on the Mechanical and Microstructural Behaviour of API X70 Steel Weldment in Seawater. M.Eng Thesis, Federal University of Technology Minna, Nigeria.

Ike, T. M., Adedipe, O., Lawal, S. A., Abolarin, M. S. & Olugboji, O. A. (2019). Investigation of the Mechanical and Microstructural Properties of Welded API X70 Pipeline Steel. *ARID Zone Journal of Engineering, Technology & Environment*, 15 (2), 342–354

Ilman, M. (2014) . Analysis of Internal Corrosion in Subsea Oil Pipeline. *Engineering Failure Analysis*, 2, 1–8

Jajja, S. A., Ali, W., Ali, H. M. & Ali, A. M. (2014). Water Cooled Minichannel Heat Sinks for Microprocessor Cooling: Effect of Fin Spacing. *Applied Thermal Engineering*, 64 (2), 76–82

Javidi, M., & Horeh, S. B. (2014). Investigating the Mechanism of Stress Corrosion Crackingin near-Neutral and High pH Environments for API 5L X52 Steel. *Corrosion Science*, 80, 213–220.

Johnson, R., Bretherton, I., Tomkins, B., Scott, P. M. & Silvester, D. R. V. (1978). The Effect of Sea Water Corrosion on Fatigue Crack Propagation in Structural Steel. Paper 15. *European Offshore Steels Research Seminar*, Cambridge, United Kingdom: The Welding Institute, Abington Hall Abington Cambridge CB16AL UK, 1980.

Kalantzis, C. (2014). Corrosion in Pipelines. MSc Thesis, Cranfield University.

Kelso, M. (2020). Pipelines Continue to Catch Fire and Explode.

Kermani, M.B. & Harrop, D. (1996). The Impact of Corrosion on Oil and Gas Industry. *Society of Petroleum Engineers,* 11 (3), 186–190. doi:http://dx.doi.org/10.2118/29784-PA.

Khazrattul Bin Bani, M. (2008). *Design and Development of a Small DC Refrigerator.* BSc Thesis, Universiti Malaysia.

Khurmi, R. S. & Gupta, J. K. (2016). *A Texbook of Refrigeration and Airconditioning*. Edited by S. Chand. Revised Ed. Eurasia Publishing House (P) LTD

Kim, C., Jong-bong, L. & Jang-yong, Y. (2005). A Study on the Metallurgical and Mechanical Characteristics of the Weld Joint of X80 Steel. *International Offshore and Polar Engineering Conference,* 8, 158–162

Leonardo, B. G., Luiz, C. C., Rodrigo, V. V. & Luiz, H. S. (2014). Microstructure and Mechanical Properties of Two API Steels for Iron Ore Pipelines. *Journal of Universidade Federal de Ouropreto,* 17, 1516–1639

Li, M. C., & Cheng, Y. F. (2008). Corrosion of the Stressed Pipe Steel in Carbonate-Bicarbonatesolution Studied by Scanning Localized Electrochemical Impedance Spectroscopy. *Electrochim Acta,* 53, 2831–2836

Little, B. & Lee, J. (2007). *Microbioligically Influenced Corrosion*. 1st ed. Hoboken, New Jersey: Wiley Interscience

Liu, C., Wang, D., Sun, Z., Chen, L., Shi, J. & Chen J. (2018). Effects of Charge on the Performance of R290 Air Conditioner with Different Expansion Devices. *Applied Thermal Engineering,* 140, 498–504

Madriya, D. M., Marangwanda, G. T., Ekundayo, F. M., Babarinde, T. O. & Akinlabi, S B. (2019). Investigation of Household Refrigerator System with Varied Capillary Tube Length. *IOP Conference Series:Journal of Physics,* 1378: 042056. doi:10.1088/1742-6596/1378/4/042056

Mogaji, T. S. (2019). Development of an Improved Vapour Compression Refrigeration System for Preservation of Fresh Vegatables. *Journal of Enginering and Engineering Technology,* 13, 1–11

Mohammadi, K. & McGowan, J. G. (2018). An Efficient Integrated Trigeneration System for the Production of Dual Temperature Cooling and Fresh Water: Thermoeconomic Analysis and Optimization. *Applied Thermal Engineering,* 145, 652–666

Muneer, B., Ehab, E., Mahmoud, S., Abdulhakim, A., Waleed, A. & Khaled, A. (2015). Mechanical Properties, Microstructure and Toughness Assessment of an X70 Pipeline Steel. *Materials Testing,* 57 (10), 897–903

Mustapha, A. (2010). The Effect of Microstructure on the Susceptibility of Pipeline Steels to Environment-Assisted Cracking. PhD Thesis, Newcastle University, United Kingdom.

Myers, P.T. (1998). *Corrosion Fatigue and Fracture Mechanics of High Strength Jack up Steels.* PhD thesis, University College London.

Naidu, D. S., Selahattin, O. & Kevin, M. (2003). Modeling, Sensing and Control of Gas Metal Arc Welding. *Science,* doi:https://doi.org/10.1016/B978-0-08-044066-8.X5000-9.

Norman, D. & Argent, C. (2007). Pipeline Coating: External Corrosion and Direct Assessment. *Corrosion Processes,*

Omale, J. I., Oheri, E. G., Tiamiyu, A. A., Eskandari, M. & Szpunar, J. A. (2017). Microstructure, Texture Evolution and Mechanical Properties of X70 Pipeline Steel after Different Thermo Mechanical Treatments. *Material Science and Engineering,* 703, 485–497

Oyedepo, S.O., Fagbenle, R. O., Babarinde, T. & Tunde, T. (2016). Effect of Capillary Tube Length and Refrigerant Charge on the Performance of Domestic Refrigerator with R12 and R600a. *International Journal of Advanced Thermofluid Research,* 2 (1), 2–14

Popoola, L.T., Grema, A. S., Latinwo, G. K. & Gutti, B. (2013). Corrosion Problems during Oil and Gas Production and Its Mitigation. *International Journal of Industrial Chemistry,* 4 (35). https://doi.org/ 10.1186/2228-5547-4-35

Ramu, N. S., Kumar, P.S. & Mohanraj, M. (2014). Energy Performance Assessment of R32 / R125 / R600a Mixtures as Possible Alternatives to R22 in Compression Refrigeration Systems. *International Journal of Mechanical and Mechatronics Engineering,* 14 (02), 12–22

Raymond, L. (1988). *Hydrogen Embrittlement. 1*st ed. Philadelphia: ASTM

Revie, R. W. (2000). Uhlig's Corrosion Handbook. Edited. New York: John Wiley & Sons

Roche, M. (2005). External Corrosion of Pipelines: What Risk?" *Corrosion Processes.*

Saibhargav, A., Reddy, K. S. & Reddy, V. M. (2019). Performance Analysis of Vapour Compression Refrigeration System Using HC Refrigerant Mixtures for Water Chiller. *International Journal of Innovative Technology and Exploring Engineering,* 8 (9), 2513–2517. doi:10.35940/ijitee.I7862.078919.

Scott, P. M., Thorpe, T. W. & Silvester, D. R. V. (1983). Rate -Determining Process for Corrosion Fatigue Crack Growth in Ferrite Steels in Seawater. *Corrosion Science,* 23 (6), 559–575.

Sedriks, A. J. (1996). *Corrosion of Stainless Steels*. 2nd ed. New York: John Wiley & Sons.

Sharma, S. K. & Maheshwari, S (2017). A Review on Welding of High Strength Oil and Gas Pipeline Steels. *Journal of Natural Gas Science and Engineering,* 38,

203–217 doi:10.1016/j.jngse.2016.12.039

Shifler, D. A. & Denise, M. A. (2005). Factors Affecting Corrosion Performance and Testing of Materials and Components in Seawater. *NACE International Corrosion Conference*, 1–15. Houston, Texas

Shifler, D. A. (2005). Understanding Material Interactions in Marine Environments to Promote Extended Structural Life. *Corrosion Science*, 47 (10), 2335–2352 doi:10.1016/j.corsci.2004.09.027

Siricharoenpanich, A., Wiriyasart, S., Prurapark, R. & Naphon, P. (2019). Effect of Cooling Water Loop on the Thermal Performance of Air Conditioning System. *Case Studies in Thermal Engineering*, 15, 100518

Song, F. M. (2009). Predicting the Mechanisms and Crack Growth Rates of Pipelinesundergoing Stress Corrosion Cracking at High pH. *Corrosion Science*, 51, 2657–2674

Sutthivirode, K. & Thongtip, T. (2020). Experimental Investigation of Vapour Compression Chiller Based on Transient Cooling Performance Influenced by Expansion Devices. *Case Studies in Thermal Engineering*, 21, 1–16. doi:10.1016/j.csite.2020.100669

Thu, K., Saththasivam, J., Saha, B. B., Chua, K. J., Murthy, S. S. & Choon Kim, N. (2017). Experimental Investigation of a Mechanical Vapour Compression Chiller at Elevated Chilled Water Temperatures. *Applied Thermal Engineering*. doi:10.1016/j.applthermaleng.2017.05.091.

Tian, Q., Cai, D., Ren, L., Tang, W., Xie, Y., He, G. & Liu, F. (2014). An Experimental Investigation of Refrigeran Mixture R32/R290 as Drop-In Replacement for HFC410A in Household Air Conditioners. *International Journal of Refrigeration*, 57, 216–228.

Ugwu, H. U. (2012). Design , Fabrication and Performance Evaluation of a Micro-Absorption Refrigerator. *International Journal of Engineering and Technology*, 2 (11), 1813–1823

Vesga Rivera, W. (2014). Structural Integrity of Steel Pipelines for CO2 Transport. PhD Thesis, Cranfield University

Wang, X., Xinghua, T., Liwei, W., Cui, W. & Zhenzhen, G. (2014). Corrosion Behavior of X80 Pipeline Steel under Coupling Effect of Stress and Stray Current 9, 4574–4588

Wang, Y., Guangxu, C., Wei, W., Qiao, Q., Yun, L. & Xiufeng, L. (2015). Effect of pH and Chloride on the Micro-Mechanism of Pitting Corrosion for High Strength Pipeline Steel in Aerated NaCl Solutions. *Applied Surface Science*, 349, 746–756 doi:10.1016/j.apsusc.2015.05.053.

Wu, J., Yang, L. & Hou, J. (2012). Experimental Performance Study of a Small Wall Room Air Conditioner Retrofitted with R290 and R1270. *International Journal of Refrigeration*, 35, 1860–1868

Yang, Y., Feng, L. & Feng, X. (2020). Tensile Fracture Behavior of Corroded Pipeline : Part 1 — Experimental Characterization. *Advances in Material Science and Engineering*,317,837-848 doi:https://doi.org/10.1155/2020/4058452.